

SALSA: Sequential Approximate Leverage-Score Algorithm with Application in Analyzing Big Time Series Data

Ali Eshragh* Luke Yerbury† Asef Nazari‡ Fred Roosta§
Michael W. Mahoney¶

Abstract

We develop a new efficient sequential approximate leverage score algorithm, SALSA, using methods from randomized numerical linear algebra (RandNLA) for large matrices. We demonstrate that, with high probability, the accuracy of SALSA’s approximations is within $(1 + \mathcal{O}(\varepsilon))$ of the true leverage scores. In addition, we show that the theoretical computational complexity and numerical accuracy of SALSA surpass existing approximations. These theoretical results are subsequently utilized to develop an efficient algorithm, named LSARMA, for fitting an appropriate ARMA model to large-scale time series data. Our proposed algorithm is, with high probability, guaranteed to find the maximum likelihood estimates of the parameters for the true underlying ARMA model. Furthermore, it has a worst-case running time that significantly improves those of the state-of-the-art alternatives in big data regimes. Empirical results on large-scale data strongly support these theoretical results and underscore the efficacy of our new approach.

1 Introduction

Leverage-scores are a statistical concept for measuring the influence of individual observations on the overall fitting of a model. They were initially used in the context of ordinary least squares (OLS) regression, but the concept was extended to other statistical models too. In that context, data points with high leverage-scores can strongly affect the estimated

*Carey Business School, Johns Hopkins University, MD, USA, and International Computer Science Institute, Berkeley, CA, USA. Email: ali.eshragh@jhu.edu

†School of Information and Physical Sciences, University of Newcastle, NSW, Australia. Email: luke.yerbury@newcastle.edu.au

‡School of Information Technology, Deakin University, Australia. Email: asef.nazari@deakin.edu.au

§School of Mathematics and Physics, University of Queensland, Australia, ARC Training Centre for Information Resilience, the University of Queensland, Australia, and International Computer Science Institute, Berkeley, CA, USA. Email: fred.roosta@uq.edu.au

¶Department of Statistics, University of California at Berkeley, USA; Lawrence Berkeley National Laboratory, Berkeley, USA; and International Computer Science Institute, Berkeley, CA, USA. Email: mmahoney@stat.berkeley.edu

coefficients of the regression model, potentially leading to skewing the model’s predictions. Nowadays, leverage-scores play multiple roles across numerous domains within data analysis and machine learning. One prime application of leverage-scores is in detecting outliers and anomalies [46], where they play an important role in identifying strange data points through the assessment of their corresponding leverage-score magnitudes. Furthermore, leverage-scores are useful in the context of dimensionality reduction [33] and the creation of sparse models [31], because they help in the selection of the most relevant features or dimensions, consequently facilitating the development of more interpretable models. In addition, they are used in recommendation systems, where they are employed to propose items showing a strong influence on users [5]. These applications highlight the multifaceted application of leverage-scores, proving their significance across a spectrum of data analysis and machine learning tasks.

In dealing with large-scale computations, especially in relation to huge data matrices and big OLS problems, randomized numerical linear algebra (**RandNLA**) has appeared as a highly effective approach [11, 14, 15, 35, 39]. This field exploits various random sub-sampling and sketching methods to manage such scenarios. Essentially, **RandNLA** involves the random yet purposeful compression of the underlying data matrix into a smaller version while preserving many of its original characteristics. This compression allows a significant portion of the resource-intensive calculations to be executed using size-reduced matrices. [35] and [50] have provided comprehensive insights into **RandNLA** subroutines and their diverse applications. Furthermore, implementations of algorithms based on these principles have demonstrated superior performance over state-of-the-art numerical methods [3, 38, 51].

Condensing a sizable matrix into a computationally manageable form through sub-sampling requires an appropriate sampling technique. Although uniform sampling methods are straightforward, they prove significantly less effective when confronted with data non-uniformity, such as outliers. In such scenarios, non-uniform yet still independently and identically distributed (i.i.d.) sampling schemes, especially sampling based on leverage-score ([13]), play an important role. They not only provide robust worst-case theoretical guarantees, but also facilitate the creation of high-quality numerical implementations.

In particular, when dealing with time series data, leverage-score-based sampling methods show a high level of efficiency in estimating the parameters of **ARMA** models. However, computing these leverage-scores can be as computationally expensive as solving the original OLS problems. In this context, employing the time series model’s inherent structure to estimate the leverage-scores appears to be a crucial determinant for the development of efficient algorithms in time series analysis. We explore this approach within the framework of **ARMA** models in this work.

This study offers the following contributions:

- (a) Applying **RandNLA** methods to develop **SALSA**, an efficient recursive algorithm for estimating leverage scores of large matrices.
- (b) Establishing a high-probability theoretical relative error bound for leverage-score estimation.
- (c) Utilizing **SALSA** to develop **LSARMA**, a novel algorithm for estimating parameters of the

ARMA model for large-scale time series data.

- (d) Providing both theoretical and empirical demonstrations of the efficiency of the proposed algorithms using both real-world and synthetic big data.

We structure the rest of this paper as follows: In Section 2, we provide essential background information about **RandNLA**, leverage-score-based sampling, and a brief literature review. Section 3 presents the theoretical insights into recursive methods for the estimation and exact computation of leverage-scores, which form the basis for **SALSA**. Section 4 gives the numerical results obtained by applying **SALSA** for estimating leverage-scores in large synthetic and real-data matrices. In Section 5, we focus on the application of **SALSA** in handling big time series data, introducing a novel algorithm known as **LSARMA**. Finally, Appendix A contains technical lemmas and their corresponding proofs.

Notation

In this paper, we adopt a notation scheme for vectors and matrices. Specifically, bold lowercase letters (\mathbf{v}) represent vectors, uppercase letters (\mathbf{M}) represent matrices, and regular lowercase letters (c) denote scalars. All vectors are column vectors, and we indicate the transpose of a vector as \mathbf{v}^\top . For real matrices \mathbf{M} , we use $\|\mathbf{M}\|$ to imply the ℓ_2 norm. Following the conventions of MATLAB, $\mathbf{M}(i, :)$ and $\mathbf{M}(:, j)$ refer to the i^{th} row and j^{th} column of matrix \mathbf{M} , respectively. Furthermore, $\mathbf{v}(i)$ denotes the i^{th} component of vector \mathbf{v} . We represent a vector with a value of one in the i^{th} component and zeros elsewhere as \mathbf{e}_i . Lastly, we represent the identity matrix of size $n \times n$ as \mathbf{I}_n , and the number of nonzero components of matrix \mathbf{M} is denoted by $\text{nnz}(\mathbf{M})$.

2 Background

2.1 Randomized Numerical Linear Algebra

This section provides an introduction to key **RandNLA** concepts, which will play a fundamental role in shaping the development of **SALSA** and its associated theoretical and numerical outcomes. **RandNLA** is an evolving field of research [11, 14, 15, 23, 35, 39], where the strategic integration of randomization techniques into traditional numerical algorithms enables the creation of more efficient algorithms suitable for linear algebra challenges in dealing with big data. These challenges pertain to a spectrum of critical tasks in linear algebra, including large matrix multiplication, low-rank matrix approximation, and solving the least-squares approximation problem [15]. Although these fundamental problems are well studied, the area of **RandNLA** offers innovative approaches that improve traditional exact methods, promising more effective solutions in terms of both speed and memory requirements when dealing with large-scale problems. For example, consider an over-determined OLS problem,

$$\min_{\mathbf{x}} \|\mathbf{A}_{m,n}\mathbf{x} - \mathbf{b}\|^2, \tag{1}$$

where $\mathbf{A}_{m,n} \in \mathbb{R}^{m \times n}$, $\mathbf{x} \in \mathbb{R}^n$ and $\mathbf{b} \in \mathbb{R}^m$.

Solving (1) using the normal equations necessitates $\mathcal{O}\left(mn^2 + \frac{n^3}{3}\right)$ flops, employing QR factorization with Householder reflections reduces this requirement to $\mathcal{O}(mn^2 - n^3)$ flops, and solving via the singular value decomposition increases it to $\mathcal{O}(mn^2 + n^3)$ flops, as detailed in [28]. Additionally, iterative solvers such as LSQR [42], LSMR [27], and LSLQ [25] require roughly $\mathcal{O}(mnc)$ flops after c iterations. However, for large-scale problems with substantially large values of m and n , the computational complexity of these algorithms worsens significantly. To mitigate this issue, when a controlled level of error bounds is acceptable, randomized approximation algorithms can substantially enhance computational efficiency by providing more favorable time-complexity outcomes.

RandNLA proposes a solution for addressing the problem presented in (1) by approximating the data matrix $\mathbf{A}_{m,n}$ through the creation of an appropriately compressed matrix. This approximation is achieved by selecting s rows from the matrix $\mathbf{A}_{m,n}$ (where $n \leq s \ll m$) with replacement, guided by a specified discrete probability distribution defined over the rows. To formalize this process, we denote the resulting smaller matrix as $\mathbf{S}_{s,m}\mathbf{A}_{m,n}$, with $\mathbf{S}_{s,m}$ belonging to $\mathbb{R}^{s \times m}$. This matrix is commonly referred to as a sketching or sampling matrix, and its construction is based on a predefined sampling procedure. The algorithms mentioned earlier for solving (1) can subsequently be employed to solve the modified problem, denoted as

$$\min_{\mathbf{x}} \|\mathbf{S}_{s,m}\mathbf{A}_{m,n}\mathbf{x} - \mathbf{S}_{s,m}\mathbf{b}\|^2. \quad (2)$$

In this problem, the originally larger dimension m has been replaced with a significantly smaller value, denoted as s . Note that matrix multiplication within (2) is computationally expensive. Therefore, algorithms applying this approach are not typically implemented exactly in this manner. However, this formulation provides a valuable tool for theoretical analysis of such algorithms, allowing us to understand their worst-case behavior and performance characteristics.

To ensure the effectiveness of this approximation, the choice of the sketching matrix $\mathbf{S}_{s,m}$ must be decided carefully. In fact, the sketching matrix should be designed in a way that guarantees the achievement of an ℓ_2 subspace embedding. This property becomes crucial when we permit a small failure probability δ , where $0 < \delta < 1$, and the value of s is sufficiently large. We can then establish the following relationship:

$$\Pr\left(\|\mathbf{A}_{m,n}\mathbf{x}^* - \mathbf{b}\|^2 \leq \|\mathbf{A}_{m,n}\mathbf{x}_s^* - \mathbf{b}\|^2 \leq (1 + \mathcal{O}(\varepsilon))\|\mathbf{A}_{m,n}\mathbf{x}^* - \mathbf{b}\|^2\right) \geq 1 - \delta, \quad (3)$$

where \mathbf{x}^* represents the solution to (1), \mathbf{x}_s^* represents the solution to (2), and $0 < \varepsilon < 1$. Subspace embeddings are fundamental to RandNLA theory and practice and were first introduced in data-aware form for least squares regression in [16] (and immediately extended to low-rank approximation in [17, 36], where the connection with leverage-scores was made explicit). They were first used in a data-oblivious form in [18, 45] and were popularized in data-oblivious form by [50].

The formulation of the sketching matrix $\mathbf{S}_{s,m}$ can be executed in various ways, broadly categorized as either data-oblivious or data-aware methods. Data-oblivious constructions involve techniques such as uniform sampling and random projection. Although uniform

sampling is a fast process requiring constant time, it performs poorly when the rows of $\mathbf{A}_{m,n}$ exhibit non-uniformity (outliers, as quantified by having large leverage-scores). To achieve the desired subspace embedding property, s should be within $\mathcal{O}(m)$, which essentially defeats the purpose of subsampling. On the other hand, random projection methods, such as the Subsampled Randomized Hadamard Transform (SRHT), aim to mitigate non-uniformity by projecting data into a subspace where uniform sampling becomes more effective. Details regarding these methods, and the required sample sizes to achieve (3) in the data-oblivious setting, can be found in [50].

Data-aware constructions, conversely, take into account the non-uniformity of the data when constructing a non-uniform sampling distribution over the rows of $\mathbf{A}_{m,n}$. Distributions employing statistical leverage-scores to describe the significance of individual rows have been demonstrated to enhance the theoretical guarantees of matrix algorithms [13] and prove highly effective in practical implementations [35], and distributions depending on generalizations of these scores lead to still further improvement in RandNLA theory and practice [11]. An interesting observation is that the most effective random projection algorithms, including SRHT, transform the data in such a manner that the leverage-scores become approximately uniformly distributed, making uniform sampling a suitable choice [13, 18, 35].

2.2 Leverage-score-based Sampling

From a statistical perspective in the context of linear regression, leverage-scores are used to identify influential data points in a dataset. They help assess the impact of individual data points on the coefficients of a regression model. In addition, the magnitude of leverage-scores can be used in identifying anomalies and outliers in conjunction with their residuals [43]. For a matrix, a leverage-score associated with a row indicates the significance of that row in spanning its row space. This intuition is obtained from the fact that the rank of a matrix can be calculated as the sum of its leverage-scores [6]. This property makes leverage-scores a valuable tool in sketching techniques because they provide a sampling mechanism that increases the likelihood of selecting rows that contain “important” information. As a consequence, this improves the ability of a subsampled matrix to preserve the information contained in the full matrix.

For a matrix $\mathbf{A}_{m,n}$ with $m \geq n$, the leverage-score associated with the i^{th} row of $\mathbf{A}_{m,n}$ is defined as

$$\ell_{m,n}(i) := \|\mathbf{Q}_{m,m}(i, :)\|^2,$$

where $\mathbf{Q}_{m,m}$ is *any* orthogonal matrix with the property $\text{range}(\mathbf{Q}_{m,m}) = \text{range}(\mathbf{A}_{m,n})$. This definition is essential because it illustrates that leverage-scores are well defined and do not rely on a specific choice of the orthogonal matrix $\mathbf{Q}_{m,m}$. A more practical definition of leverage-scores is derived from the concept of a hat matrix. The hat matrix for the matrix $\mathbf{A}_{m,n}$ is defined as

$$\mathbf{H}_{m,m} := \mathbf{A}_{m,n}(\mathbf{A}_{m,n}^\top \mathbf{A}_{m,n})^{-1} \mathbf{A}_{m,n}^\top. \quad (4)$$

In this setting, the leverage-score of the i^{th} row of $\mathbf{A}_{m,n}$ is the i^{th} diagonal entry of the hat

matrix, which is expressed as

$$\ell_{m,n}(i) := \mathbf{e}_i^\top \mathbf{H}_{m,m} \mathbf{e}_i, \quad \text{for } i = 1, \dots, m. \quad (5)$$

The leverage-scores of rows of a matrix can be used to construct a distribution for sampling over the rows of that matrix. In the following definition for $\mathbf{A}_{m,n}$,

$$\pi_{m,n}(i) := \frac{\ell_{m,n}(i)}{n}, \quad \text{for } i = 1, \dots, m, \quad (6)$$

as $\ell_{m,n}(i) > 0 \forall i$ and $\sum_{i=1}^m \ell_{m,n}(i) = n$. We conclude that $\pi_{m,n}(i) > 0 \forall i$ and $\sum_{i=1}^m \pi_{m,n}(i) = 1$, and we obtain a distribution based on leverage-scores. Using this distribution, one can construct the sketching matrix $\mathbf{S}_{s,m}$ by sampling (with replacement) rows of the $m \times m$ identity matrix \mathbf{I}_m according to the distribution (6). Each selected row i is scaled by a multiplicative factor

$$\frac{1}{\sqrt{s\pi_{m,n}(i)}}, \quad (7)$$

to ensure

$$\mathbb{E} [\|\mathbf{S}_{s,m} \mathbf{A}_{m,n} \mathbf{x}\|^2] = \|\mathbf{A}_{m,n} \mathbf{x}\|^2 \quad \forall \mathbf{x},$$

which guarantees unbiased solution estimates [15]. In (7), s is the number of sampled rows.

Obviously, obtaining the leverage-scores *exactly* is computationally expensive, requiring the same amount of resources in solving the original OLS problem. However, they can be computed *approximately* more quickly [13], basically in the time it takes to implement a random projection. Additionally, as highlighted in [15, 35], even with inaccurately estimated leverage-scores by a factor $0 < \beta \leq 1$ expressed as

$$\hat{\ell}(i) \geq \beta \ell(i), \quad \text{for } i = 1, 2, \dots, m,$$

we can still achieve the subspace embedding property (3) with a sample size s as given by

$$s \in \mathcal{O} \left(n \log(n/\delta) / (\beta \varepsilon^2) \right). \quad (8)$$

Equation (8) shows that a larger sample size is required when β is smaller, reflecting poorer estimates. Furthermore, if the goal is to reduce the error (ε), the sample size must be increased accordingly.

2.3 Related Work

Calculating leverage-scores for an arbitrary tall and thin data matrix $\mathbf{A}_{m,n}$, when m is significantly larger than n , through naïve algorithms based on orthogonal bases for the matrix's column space, requires a huge computational load. This computational process needs

$\mathcal{O}(mn^2)$ time, which not only proves to be computationally expensive but also contradicts the intention of using sampling techniques to reduce computational overhead. To address computational challenges in computing leverage-scores, numerous studies have been conducted to develop non-trivial and inventive methods for approximating them. One of the pioneering works to approximate leverage-scores can be found in [13]. This approach uses a rapid Johnson-Lindenstrauss mapping technique to transform a collection of high-dimensional data points into a lower-dimensional space while conserving the pairwise distances among these points. Specifically, the mapping takes the shape of a subsampled randomized Hadamard transform and plays a central role in designing a randomized algorithm for approximating leverage-scores within ε -relative accuracy in $\mathcal{O}(mn\varepsilon^{-2}\log m)$ time. Subsequent research has further enhanced this bound, mostly with respect to input sparsity [8, 37, 41, 48]. In particular, the bound was improved to $\mathcal{O}(\varepsilon^{-2}\text{nnz}(\mathbf{A}_{m,n})\log m)$, which is essentially the optimal bound attainable considering factors such as logarithmic terms [48].

Iterative sampling algorithms aimed at approximating leverage-scores have attracted attention in this domain as well [9, 32]. In [32], the authors adopt an iterative approach that alternates between the calculation of a short matrix estimate of $\mathbf{A}_{m,n}$ and the computation of increasingly accurate approximations for the leverage-scores. This iterative process results in a runtime of $\mathcal{O}(\text{nnz}(\mathbf{A}_{m,n}) + n^{\omega+\theta}\varepsilon^{-2})$, where $\theta > 0$ and $n^{\omega+\theta}$ is similar to the computational complexity of solving a regression problem on reduced matrices. Additionally, an iterative row sampling algorithm for matrix approximation is proposed in [9], emphasizing the preservation of the row structure and sparsity in the original data matrix. This study focuses on a comprehensive examination of the information loss when employing uniform sampling in the context of solving regression problems. Their findings lead to the conclusion that by appropriately assigning weights to a small subset of rows, minimizing the coherence becomes feasible, represented by the largest leverage-score, for any arbitrary matrix. Furthermore, they demonstrate the possibility of achieving constant-factor approximations of leverage-scores, where $\ell(i) \leq \hat{\ell}(i) \leq n^\theta \ell(i)$ holds for $i = 1, 2, \dots, m$, and this approximation can be computed in $\mathcal{O}(\text{nnz}(\mathbf{A}_{m,n})/\theta)$ time.

We should note quantum-inspired methods for approximating leverage-scores have been studied as well [34, 52]. In [34], the authors propose an efficient quantum algorithm suitable for least-squares regression problems involving sparse and well-conditioned matrix $\mathbf{A}_{m,n}$. For matrices that are ill conditioned or do not possess full column rank, their approach integrates regularization techniques such as ridge regression and δ -truncated singular value decomposition. This quantum-inspired technique enables the approximation of leverage-scores within ε -absolute error, in $\mathcal{O}(\text{nnz}(\mathbf{A}_{m,n})^2(m\varepsilon)^{-1}\log m)$ time. In another quantum-inspired approach for approximating leverage-scores, as introduced in [52], the method relies upon certain natural sampling assumptions. Their technique involves the computation of singular values and their corresponding right singular vectors from a compact submatrix. The results of this step are used in approximating the left singular matrix, ultimately enabling the approximation of the leverage-scores.

Lastly, note a closely related line of research is dedicated to approximating an extension of leverage-scores called ridge leverage-scores in the context of kernel ridge regression. To

effectively reduce the dimensionality of data matrices in kernel-based methods, such as kernel ridge regression using leverage-score-based distributions, Alaoui and Mahoney present a method that offers rapid approximations of ridge leverage-scores using random projections in [2]. Furthermore, Cohen et al. demonstrated in [10] that by using the monotonic property of ridge leverage-scores, approximating them using a relatively large uniform subsample of columns of matrix $\mathbf{A}_{m,n}$ is possible. Additionally, ridge leverage-scores are used in the development of a fast recursive sampling scheme for kernel Nyström approximation [40]. Other uses of leverage-scores when the data matrix is positive definite for kernel ridge regression are reported in [44] and [7].

3 SALSA: Theoretical Results

In this section, we provide the theoretical foundation and employ tools from **RandNLA** to support the creation of a recursive algorithm aimed at approximating the leverage-scores associated with the rows of any arbitrary matrix. The algorithm is called **SALSA**. More specifically, we start by introducing a recursive approach for the exact computation of leverage-scores of the matrix’s rows. Then, we present a complementary approximate recursion that forms the foundation of **SALSA**. It is theoretically proved that estimates from **SALSA** have desirable relative error bounds with high probability.

3.1 A Recursive Procedure for Exact Leverage-Scores

To explain the central theorem regarding a recursive approach for computing the exact leverage-scores of a data matrix, we describe a column-wise matrix augmentation procedure. This procedure starts with the first column and incrementally incorporates additional columns one by one until the entire matrix is reconstructed. This procedure is similar to the one devised in [24]; however, it does not rely on any predefined structure for the original matrix. From the original matrix $\mathbf{A}_{m,n}$, suppose we have already constructed the following submatrix:

$$\mathbf{A}_{m,d} = (\mathbf{a}_0 \mid \mathbf{a}_1 \mid \cdots \mid \mathbf{a}_{d-1}), \quad (9)$$

where $\mathbf{a}_0 = \mathbf{A}_{m,n}(:, 1) \in \mathbb{R}^{m \times 1}$, and the first column of \mathbf{A} , and $\mathbf{a}_1, \dots, \mathbf{a}_{d-1}$ are the next $d - 1$ columns in the same order they appear in the matrix. The next submatrix, $\mathbf{A}_{m,d+1}$, is constructed from $\mathbf{A}_{m,d}$ by adding the d^{th} column of $\mathbf{A}_{m,n}$ to the end of $\mathbf{A}_{m,d}$:

$$\mathbf{A}_{m,d+1} = \left(\mathbf{A}_{m,d} \mid \mathbf{a}_d \right). \quad (10)$$

Now, suppose $\phi_{m,d} \in \mathbb{R}^{d \times 1}$ is the optimal solution for the OLS problem $\min_{\phi} \|\mathbf{A}_{m,d}\phi - \mathbf{a}_d\|$, which is analytically described using the normal equation

$$\phi_{m,d} = (\mathbf{A}_{m,d}^{\top} \mathbf{A}_{m,d})^{-1} \mathbf{A}_{m,d}^{\top} \mathbf{a}_d. \quad (11)$$

Accordingly, the associated residual vector $\mathbf{r}_{m,d}$ is defined as

$$\mathbf{r}_{m,d} = \mathbf{A}_{m,d}\boldsymbol{\phi}_{m,d} - \mathbf{a}_d. \quad (12)$$

With the provided matrix augmentation procedure, the following theorem describes the recursive computation of leverage-scores of an augmented matrix using the leverage-scores of its preceding submatrix.

Theorem 1 (Recursive Scheme for Exact Leverage-Scores). *Consider the matrix $\mathbf{A}_{m,d-1}$ as in (9) and (10) ($m > d$) and its corresponding leverage-scores $\ell_{m,d-1}(i)$ for $i = 1, \dots, m$. Then the leverage-scores of the augmented matrix $\mathbf{A}_{m,d}$ can be computed as*

$$\ell_{m,d}(i) = \ell_{m,d-1}(i) + \frac{(\mathbf{r}_{m,d-1}(i))^2}{\|\mathbf{r}_{m,d-1}\|^2},$$

for $d \geq 1$, and $i = 1, \dots, m$, where $\mathbf{r}_{m,d}$ is defined in (12) and $\ell_{m,1}(i) = \frac{(\mathbf{a}_0(i))^2}{\|\mathbf{a}_0\|^2}$ for $i = 1, \dots, m$.

The recursion depicted in Theorem 1 computes the leverage-scores of $\mathbf{A}_{m,d}$ as the summation of the leverage-scores of $\mathbf{A}_{m,d-1}$ and those for the associated residual vector $\mathbf{r}_{m,d-1}$. Also, a leverage-score-based sampling distribution for every $\mathbf{A}_{m,d}$ can be constructed as follows:

$$\pi_{m,d}(i) := \frac{\ell_{m,d}(i)}{d} \quad \text{for } i = 1, \dots, m. \quad (13)$$

3.2 A Recursive Procedure for Approximate Leverage-Score

A direct application of Theorem 1 proposes an elegant but computationally expensive method for computing a matrix's leverage-scores. However, employing this recursion involves sequentially solving multiple OLS problems, demanding $\mathcal{O}(mn^3)$ flops, in contrast to the direct computation via the hat matrix, which requires $\mathcal{O}(mn^2)$ flops. To address this computational discrepancy, we introduce matrix sketching into the recursive scheme. This enhancement involves the use of two distinct instances of sketching, as follows:

- (a) when solving the OLS problem to compute $\boldsymbol{\phi}_{m,d}$ as defined in (11); and
- (b) when performing matrix multiplication to calculate $\mathbf{r}_{m,d}$ as defined in (12).

For further clarification, the first application of sketching in (a) involves reducing the number of rows in the matrix $\mathbf{A}_{m,d}$ through a sampling process to produce $\hat{\mathbf{A}}_{m,d} := \mathbf{S}_{s_1,m}^{(1)}\mathbf{A}_{m,d}$. Here, $\mathbf{S}_{s_1,m}^{(1)} \in \mathbb{R}^{s_1 \times m}$ represents a sampling matrix with s_1 rows randomly chosen with replacement from the rows of the $m \times m$ identity matrix \mathbf{I}_m . The selection of rows follows the distribution $\{\pi_{m,d}(i)\}_{i=1}^m$ outlined in (13), rescaled by the appropriate factor, as described in (7). In Definition 1, Theorem 4 replaces this distribution with one that incorporates approximate leverage-scores. An estimation of $\boldsymbol{\phi}_{m,d}$ is represented by $\hat{\boldsymbol{\phi}}_{m,d}$, which is defined as

$$\hat{\phi}_{m,d} := (\hat{\mathbf{A}}_{m,d}^\top \hat{\mathbf{A}}_{m,d})^{-1} \hat{\mathbf{A}}_{m,d}^\top \hat{\mathbf{a}}_d, \quad (14)$$

where $\hat{\mathbf{a}}_d := \mathbf{S}_{s_1,m}^{(1)} \mathbf{a}_d$. With this approximation, the approximate residual vector is given by

$$\hat{\mathbf{r}}_{m,d} := \mathbf{A}_{m,d} \hat{\phi}_{m,d} - \mathbf{a}_d. \quad (15)$$

Furthermore, for larger values of d , an additional approximation can be applied to $\mathbf{A}_{m,d} \hat{\phi}_{m,d}$ to achieve better computational efficiency. This approximation can be accomplished by employing the BasicMatrixMultiplication algorithm (of [12]), which forms the foundation for the second application of sketching mentioned in (b).

Following this algorithm, the number of columns in the matrix $\mathbf{A}_{m,d}$ is further reduced through a sampling process, resulting in $\hat{\hat{\mathbf{A}}}_{m,d} := \mathbf{A}_{m,d} \mathbf{S}_{d,s_2}^{(2)}$. In this context, $\mathbf{S}_{d,s_2}^{(2)} \in \mathbb{R}^{d \times s_2}$ represents the sampling matrix, with s_2 columns randomly selected with replacement from the columns of the \mathbf{I}_d matrix. The selection of columns follows the distribution defined by the leverage-scores of $\hat{\phi}_{m,d}$. Subsequently, a new estimate for the residual vector is obtained through

$$\hat{\hat{\mathbf{r}}}_{m,d} := \hat{\hat{\mathbf{A}}}_{m,d} \hat{\phi}_{m,d} - \mathbf{a}_d, \quad (16)$$

where

$$\hat{\phi}_{m,d} := \mathbf{S}_{d,s_2}^{(2)\top} \hat{\hat{\phi}}_{m,d}. \quad (17)$$

Note that when dealing with values of $d < s_2$, the entire matrix $\mathbf{A}_{m,d}$ is used without any sampling. In other words, $\mathbf{S}_{d,s_2}^{(2)} = \mathbf{I}_d$ for these cases. However, when $d \geq s_2$, we introduce the sketching process as described earlier.

The approximate algorithm constructed from this procedure, as outlined in Algorithm 1, demands $\mathcal{O}(mn(s_1^2 + s_2))$ flops. Furthermore, the relative error associated with this algorithm can be favorably bounded a priori. In what follows, we introduce key theorems that establish this relative error bound and provide a comprehensive definition of the algorithm and its components.

The following theorem provides bounds for the estimates presented in (14) and (15).

Theorem 2 ([18]). *Let $0 < \varepsilon_1, \delta < 1$. For sampling with (approximate) leverage-scores, using a sample size s as described in (8), the following inequalities hold with a probability of at least $1 - \delta$:*

$$\begin{aligned} \|\mathbf{r}_{m,d}\| &\leq \|\hat{\mathbf{r}}_{m,d}\| \leq (1 + \varepsilon_1) \|\mathbf{r}_{m,d}\|, \\ \|\phi_{m,d} - \hat{\phi}_{m,d}\| &\leq \sqrt{\varepsilon_1} \eta_{m,d} \|\phi_{m,d}\|, \end{aligned}$$

where $\phi_{m,d}$, $\mathbf{r}_{m,d}$, $\hat{\phi}_{m,d}$, and $\hat{\mathbf{r}}_{m,d}$ are defined respectively in (11), (12), (14), and (15). Additionally,

$$\eta_{m,d} = \kappa(\mathbf{A}_{m,d}) \sqrt{\zeta^{-2} - 1},$$

where $\kappa(\mathbf{A}_{m,d})$ represents the condition number of matrix $\mathbf{A}_{m,d}$, and $\zeta \in (0, 1]$ denotes the fraction of \mathbf{a}_d lying within $\text{Range}(\mathbf{A}_{m,d})$. In other words, ζ is defined as

$\zeta := \|\mathbf{H}_{m,m}\mathbf{a}_d\|/\|\mathbf{a}_d\|$ with $\mathbf{H}_{m,m}$ is the hat matrix corresponding to $\mathbf{A}_{m,d}$.

Next, we present Theorem 3, which appears as a consequence of Theorem 1 in [12]. This theorem provides bounds for the estimates produced by the BasicMatrixMultiplication algorithm (of [12]). This algorithm is a sampling-based approach aimed at approximating the product of two large matrices while preserving the dimensionality of the resulting product. This randomized matrix multiplication algorithm plays an important role in various other RandNLA algorithms. Let's consider two matrices, $\mathbf{A}_{m,n} \in \mathbb{R}^{m \times n}$ and $\mathbf{B}_{n,p} \in \mathbb{R}^{n \times p}$. The multiplication between them is defined as

$$\mathbf{A}_{m,n}\mathbf{B}_{n,p} = \sum_{t=1}^n \mathbf{A}_{m,n}(:,t)\mathbf{B}_{n,p}(t,:).$$

This summation involves the addition of n rank-one matrices, each of which results from the outer product of a column from matrix $\mathbf{A}_{m,n}$ and a row from matrix $\mathbf{B}_{n,p}$. These rank-one matrices have the same dimensionality of $m \times p$ as the product matrix. The outer product characteristic creates an opportunity to approximate this product using a reduced number of rank-one matrices. This reduction is achieved by carefully selecting (with replacement) corresponding columns and rows from matrices $\mathbf{A}_{m,n}$ and $\mathbf{B}_{n,p}$ based on a given probability distribution, scaled as follows:

$$\sum_{t=1}^c \frac{1}{c\pi_{i_t}} \mathbf{A}_{m,n}(:,i_t)\mathbf{B}_{n,p}(i_t, :).$$

Here, $i_t \in \{1, \dots, n\}$ is chosen such that $\Pr(i_t = k) = \pi_k$. This approach allows for efficient matrix multiplication approximations while reducing computational burden.

Theorem 3 ([12]). Consider matrices $\mathbf{A}_{m,n} \in \mathbb{R}^{m \times n}$ and $\mathbf{B}_{n,p} \in \mathbb{R}^{n \times p}$, and a positive integer c such that $1 \leq c \leq n$. Let $\{\pi_i\}_{i=1}^n$ be a set of non-negative scalars satisfying $\sum_{i=1}^n \pi_i = 1$, and for a positive constant $\beta \leq 1$, let them also satisfy the condition

$$\pi_i \geq \frac{\beta \|\mathbf{A}_{m,n}(:,i)\| \|\mathbf{B}_{n,p}(i,:)\|}{\sum_{k=1}^n \|\mathbf{A}_{m,n}(:,k)\| \|\mathbf{B}_{n,p}(k,:)\|}.$$

We define $\mathbf{C}_{m,c}\mathbf{R}_{c,p}$ as the approximation to the matrix product $\mathbf{A}_{m,n}\mathbf{B}_{n,p}$ obtained using the BasicMatrixMultiplication algorithm (of [12]). If c satisfies the condition $c \geq \xi^2/(\beta\varepsilon_2^2)$, we can establish, with a probability of at least $1 - \delta$, the following inequality:

$$\|\mathbf{A}_{m,n}\mathbf{B}_{n,p} - \mathbf{C}_{m,c}\mathbf{R}_{c,p}\|_F \leq \varepsilon_2 \|\mathbf{A}_{m,n}\|_F \|\mathbf{B}_{n,p}\|_F,$$

where $\xi = 1 + \sqrt{(8/\beta) \log(1/\delta)}$.

Theorem 3 shows that by sampling a sufficient number of column-row pairs, the approximation error $\|\mathbf{A}_{m,n}\mathbf{B}_{n,p} - \mathbf{C}_{m,c}\mathbf{R}_{c,p}\|_F$ can be reduced to arbitrary precision. Now, we proceed to introduce the recursive procedure for approximating the leverage-scores in Definition 1. This recursive procedure is analogous to the exact one presented in Theorem 1, using the two instances of matrix sketching previously described.

Definition 1 (Sequential Approximate Leverage-Scores). *Consider matrix $\mathbf{A}_{m,d}$ defined recursively as $\mathbf{A}_{m,d+1} = \left(\mathbf{A}_{m,d} \mid \mathbf{a}_d\right)$. The sequential approximate leverage-scores are defined by the following recursion:*

$$\hat{\ell}_{m,d}(i) := \begin{cases} \ell_{m,1}(i), & \text{for } d = 1, \\ \hat{\ell}_{m,d-1}(i) + \frac{(\hat{\mathbf{r}}_{m,d-1}(i))^2}{\|\hat{\mathbf{r}}_{m,d-1}\|^2}, & \text{for } 2 \leq d \leq s_2, \\ \hat{\ell}_{m,d-1}(i) + \frac{(\hat{\mathbf{r}}_{m,d-1}(i))^2}{\|\hat{\mathbf{r}}_{m,d-1}\|^2}, & \text{for } d > s_2, \end{cases}$$

where $\hat{\mathbf{r}}_{m,d-1}$ and $\hat{\mathbf{r}}_{m,d-1}$ are given in (15) and (16), respectively.

We now introduce SALSA as outlined in Algorithm 1. This algorithm is designed to provide approximate leverage-scores for any matrix $\mathbf{A}_{m,n} \in \mathbb{R}^{m \times n}$. Theorem 4 describes the relative error associated with the leverage-score estimates produced by this algorithm.

Theorem 4 (Relative Errors for Sequential Approximate Leverage-Scores). *When computing the approximate leverage-scores, as defined in Definition 1, if the row-sketch of size s_1 is performed based on the leverage-score sampling distribution,*

$$\hat{\pi}_{m,d}(i) = \frac{\hat{\ell}_{m,d}(i)}{d} \quad \text{for } i = 1, \dots, m,$$

and the column-sketch of size s_2 is performed based on the leverage-score distribution

$$\hat{\hat{\pi}}_{m,d}(i) = \frac{(\hat{\phi}_{m,d}(i))^2}{\|\hat{\phi}_{m,d}\|^2} \quad \text{for } i = 1, \dots, d,$$

we can establish, with a probability of at least $1 - \delta$, the following inequality:

$$\frac{|\ell_{m,d}(i) - \hat{\ell}_{m,d}(i)|}{\ell_{m,d}(i)} \leq (\sqrt{\xi_{m,d-1}} + 5(\eta_{m,d-1} + 2)\kappa^2(\mathbf{A}_{m,d}))(d-1)\sqrt{\varepsilon^*},$$

Algorithm 1 SALSA: Sequential Approximate Leverage-Scores Algorithm

Input:

- Matrix $\mathbf{A}_{m,d} = (\mathbf{a}_0 \mid \mathbf{a}_1 \mid \cdots \mid \mathbf{a}_{d-1}) \in \mathbb{R}^{m \times n}$ as in (9);

Step -1. Set s_2 as in Theorem 3, replacing c with s_2 ;

Step 0. Set $d = 1$ and $\mathbf{A}_{m,d} = \mathbf{a}_{d-1}$;

while $d < n$ **do**

Step 1. Compute the approximate leverage-scores $\hat{\ell}_{m,d}(i)$ for $i = 1, \dots, m$ as in Definition 1;

Step 2. Compute the sampling distribution $\hat{\pi}_{m,d}(i)$ for $i = 1, \dots, m$ as in (13);

Step 3. Set s_1 as in (8) by replacing n with d ;

Step 4. Form the $s_1 \times m$ sampling matrix $\mathbf{S}_{s_1,m}^{(1)}$ by randomly choosing s_1 rows of the corresponding identity matrix according to the probability distribution found in Step 3, with replacement, and rescaling them with the factor (7);

Step 5. Construct the sampled matrix $\hat{\mathbf{A}}_{m,d} = \mathbf{S}_{s_1,m}^{(1)} \mathbf{A}_{m,d}$ and response vector $\hat{\mathbf{a}}_d = \mathbf{S}_{s_1,m}^{(1)} \mathbf{a}_d$;

Step 6. Solve the associated reduced OLS problem to find the parameters $\hat{\phi}_{m,d}$ as in (14);

Step 7. If $d \leq s_2$, set $\mathbf{S}_{d,s_2}^{(2)} = I_{d,d}$ and go to Step 10;

Step 8. Compute the sampling distribution $\hat{\pi}_{m,d}(i)$ for $i = 1, \dots, d$ as in Theorem 4;

Step 9. Form the $d \times s_2$ sampling matrix $\mathbf{S}_{d,s_2}^{(2)}$ by randomly choosing s_2 columns of the corresponding identity matrix according to the probability distribution found in Step 7, with replacement, and rescaling them with the factor (7);

Step 10. Construct the sampled matrix $\hat{\mathbf{A}}_{m,d} = \mathbf{A}_{m,d} \mathbf{S}_{d,s_2}^{(2)}$ and estimated parameters $\hat{\phi}_{m,d} = \mathbf{S}_{d,s_2}^{(2)\top} \hat{\phi}_{m,d}$;

Step 11. Calculate the residuals $\hat{\mathbf{r}}_{m,d}$ as in (17);

Step 12. Set $\mathbf{A}_{m,d+1} = (\mathbf{A}_{m,d} \mid \mathbf{a}_d)$ and $d \leftarrow d + 1$;

end while

Step 13. Compute the approximate leverage-scores $\hat{\ell}_{m,d}(i)$ for $i = 1, \dots, m$ as in Definition 1;

Output: Estimated leverage-scores $\hat{\ell}_{m,n}(i)$ for $i = 1, \dots, m$.

for $i = 1, \dots, m$, where

$$\xi_{m,d-1} = 1 + 2\kappa(\mathbf{A}_{m,d-1})\sqrt{d-1},$$

and $\eta_{m,d}$ and $\kappa(\mathbf{A}_{m,d})$ are as in Theorem 2 and $\varepsilon^* = \max\{\varepsilon_1, \varepsilon_2\}$. Note ε_1 is defined in Theorem 2 and ε_2 is defined in Theorem 3.

4 SALSA: Numerical Results

In this section, we present the numerical results that demonstrate the efficiency of SALSA in estimating leverage-scores. The numerical experiments were conducted using MATLAB R2022a on a Windows machine equipped with an Intel(R) Xeon(R) CPU @3.60GHz 6 cores. To ensure fair comparisons and consistency, all computations are performed using a single thread in MATLAB, despite the multi-core capacity of the device for parallel computing.

4.1 Synthetic Big Data

To compare the performances of exact leverage-score calculations using (4) with the estimation method implemented in SALSA, we conducted numerical experiments on a synthetic matrix $\mathbf{A}_{m \times n}$, with $m = 20,000,000$ rows and $n = 300$ columns. The entries of this matrix were generated from a standard Gaussian distribution. To introduce outliers, we randomly selected 2,000 rows and modified them. We adjusted these outlier rows by adding random numbers generated from a t -distribution with one degree of freedom, multiplied by a scalar to make them different from the original (normal) rows. The inclusion of these outliers allows us to assess the algorithm’s capability to handle non-uniformity effectively, as expected. The distribution of leverage-scores of one of these data matrices is depicted in Figure 1, which shows the non-uniformity included in the synthetic data matrix.

Following Algorithm 1 for estimating leverage-scores using SALSA, one needs to specify s_1 , the row-sketch size for the OLS step, and s_2 , the column-sketch size for the matrix/vector multiplication involved in calculating the residual vector. Hence, we investigate the impact of different choices of s_1 and s_2 on the execution time in estimating the leverage-scores and on the amount of deviation from the exact leverage-scores. In this experiment, we consider $s_1 \in \{0.005n, 0.001n, 0.002n, 0.004n\}$ and $s_2 \in \{1, 2, 4, 8\}$. For each choice of s_1 and s_2 , Figure 2 records and depicts the average time and mean absolute percentage error (MAPE) of fifty independent runs. The MAPE between exact and estimated leverage-scores is calculated as follows:

$$\text{MAPE} = \frac{1}{m} \sum_{i=1}^m \left| \frac{\ell_{m,n}(i) - \hat{\ell}_{m,n}(i)}{\ell_{m,n}(i)} \right| \times 100\%. \quad (18)$$

Employing exact methods, such as (4), for computing leverage-scores demands substantial CPU time and RAM capacity, posing a significant obstacle for numerical experiments on standard computers. The computational cost of the exact method (4) is evident in Figures 2a and 2b when compared with the SALSA estimation method presented in this work.

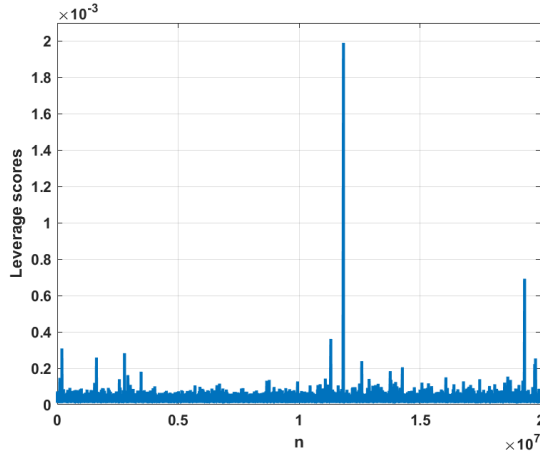
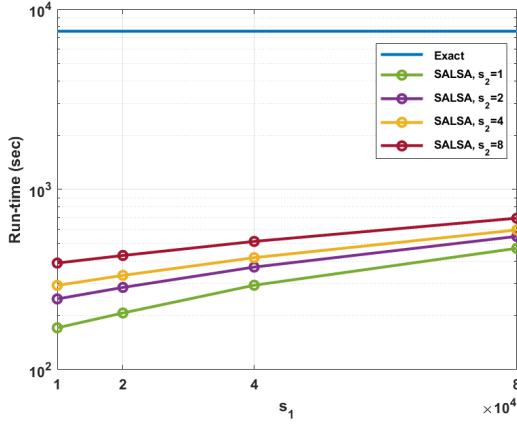


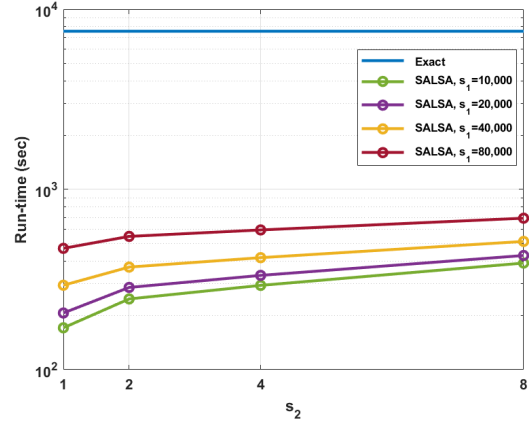
Figure 1: Non-uniform distribution of leverage-scores of the synthetic matrix with $m = 20,000,000$ rows and $n = 300$ columns, deliberately altered to include 2,000 outliers.

In our experiments with synthetic data, finding exact leverage-scores using (4) with single-threaded computations in MATLAB takes approximately 7,557 seconds, equivalent to nearly two hours. Furthermore, a matrix with 20 million rows and 300 columns requires 45 GB of memory for storage. Using the most efficient approach for computing exact leverage-scores, by using QR decomposition, necessitates an additional 95 GB of memory. Consequently, the exact method demands a total of 140 GB of memory to successfully execute. However, by employing SALSA, as described in Algorithm 1, an extensive amount of RAM is not necessary. The error bounds demonstrate the estimated and exact leverage-scores are remarkably similar, with a MAPE consistently less than 6% in the worst-case scenario as demonstrated in Figures 2c and 2d. This finding substantiates the practicality and accuracy of SALSA in estimating leverage-scores while circumventing the computational challenges associated with exact methods.

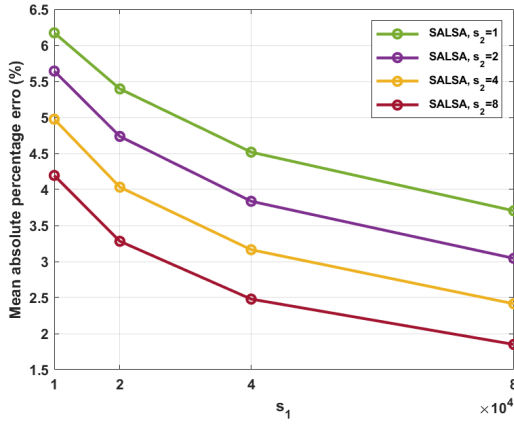
Regarding the execution-time comparison, Figure 2a clearly illustrate that as s_1 increases, regardless of the value of s_2 , SALSA needs to solve larger OLS problems, resulting in increased computational time. However, even in the worst-case scenario, the algorithm only requires 692 seconds, which is a remarkable eleven times faster than the exact method. Moreover, in the average case, SALSA completes in just 392 seconds, making it 19 times quicker than the time required for the exact method to compute the leverage-scores. This substantial reduction in computational time showcases the efficiency of SALSA in handling large-scale problems. Furthermore, similar behavior is observed for changes in s_2 in Figure 2b. For each fixed value of s_1 , as the value of s_2 increases, the execution time for SALSA increases only slightly. Figures 2a and 2b indicate that when s_1 and s_2 reach their highest values, as expected, SALSA needs to solve larger OLS problems, resulting in slightly longer execution times. Nevertheless, the differences in execution times between the highest and lowest values of s_1 and s_2 are negligible, further validating the consistent performance of SALSA across various scenarios.



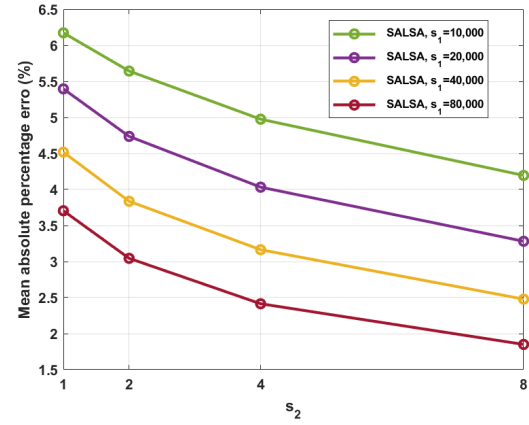
(a)



(b)



(c)



(d)

Figure 2: (2a) shows the run times as a function of s_1 for different values of s_2 for computing both exact and estimated leverage-scores, while (2b) displays the run times as a function of s_2 for different fixed values of s_1 . These results are obtained for a synthetic matrix with $m = 20,000,000$ rows and $n = 300$ columns, deliberately altered to include 2,000 outliers. Furthermore, (2c) presents the MAPE against s_1 , and (2d) depicts the same error metric against s_2 between the exact and estimated leverage-scores.

The SALSA not only estimates leverage-scores in a remarkably short time, but also maintains low error bounds on the estimations. By selecting appropriate values for s_1 and s_2 , SALSA efficiently extracts manageable-sized OLS problems from the original problem, which is solved using the exact algorithm. Despite some information being neglected in the sketching process, Figures 2c and 2d clearly demonstrate the mean percentage deviation of the estimated leverage-scores from the exact leverage-scores remains below 6%. Furthermore, in Figure 2c, with a fixed value of s_2 , as s_1 increases and SALSA incorporates more data, the deviation error decreases, indicating the algorithm's ability to produce more accurate results

as it processes additional information. Similar behavior is observed in Figure 2d when s_2 increases with a fixed value of s_1 . Even when s_1 and s_2 are at their highest values, resulting in larger OLS problems, the percentage deviations remain at the lowest levels. Additionally, the difference between the MAPE when s_1 and s_2 are at their highest and lowest values is only about 3%, further affirming the consistency and reliability of SALSA across different scenarios.

Figure 2 provides clear evidence of the remarkable efficiency of the SALSA algorithm in estimating leverage-scores. As s_1 and s_2 increase, the algorithm acquires more data and solves progressively larger problems, resulting in longer execution times but lower percentage deviations. Notably, the figure indicates the differences in execution times and deviation errors between assigning the highest or lowest values to s_1 and s_2 are not substantial. This observation highlights a trade-off between two competing objectives: the level of deviation from the exact leverage-scores and the execution time.

Setting $s_1 = 0.002n$ and $s_2 = 4$ indeed establishes a balance point where both the percentage deviation from the exact solution and the execution time reach a moderate level. This configuration proposes a well-balanced compromise, achieving reasonably accurate leverage-score estimates while keeping the computational overhead at a manageable size. In particular, with this setting, estimating the leverage-scores of a data matrix with dimensions of $20M \times 300$ takes only 293 seconds (about five minutes), and the MAPE deviation is at most 5%. This remarkable result stands in contrast to the alternative of 7,557 seconds (nearly two hours) required for exact calculations. Additionally, the advantage of not requiring a huge amount of RAM capacity further enhances the practicality and efficiency of SALSA in numerical experiments.

SALSA introduces a new level of practicality for time series analysis, enabling it to be implemented on small devices such as smartphones and wearable technologies. This advancement opens up possibilities for performing health data or market data analysis directly on these devices. With the capability of fitting good models to the data and making trustworthy predictions, SALSA empowers users to engage in data-driven decision-making and gain valuable insights without relying on resource-intensive computing systems. This integration of time series analysis on portable devices enhances convenience, accessibility, and efficiency for a wide range of applications, contributing to improved health monitoring, personalized recommendations, and smarter financial strategies.

4.2 Real-World Big Data

The real-data matrix used in our study is derived from a data matrix associated with a large knowledge graph used for hypothesis generation in the field of medical studies. In the medical and biomedical sciences, the ability to uncover implicit relationships among various concepts for rapid hypothesis generation is important. Sybrandt et al.’s seminal work [49] made a remarkable contribution to this domain. They assembled an extensive dataset comprising more than 24.5 million documents, encompassing scientific papers, keywords, genes, proteins, diseases, and diagnoses. Their work involved the development of a method for constructing a comprehensive network of public knowledge and implementing a query process capable of

revealing human-readable relationships between nodes in this network. For this purpose, they constructed a substantial graph from these objects, with 30,239,687 nodes, 4,023,336 explicitly specified zero edges, and 3,106,164 duplicate edges. The edge weights within this graph were recorded in a square data matrix, containing 30,239,687 rows and columns, with approximately 6,669,254,694 nonzero elements. We extracted a data matrix of size $m = 20,000,000$ rows and $m = 160$ from the weight matrix of the knowledge graph. The distribution of leverage-scores of this matrix is depicted in Figure 3, which shows the non-uniformity in the data matrix. For the large real-data matrix, the exact leverage-scores are

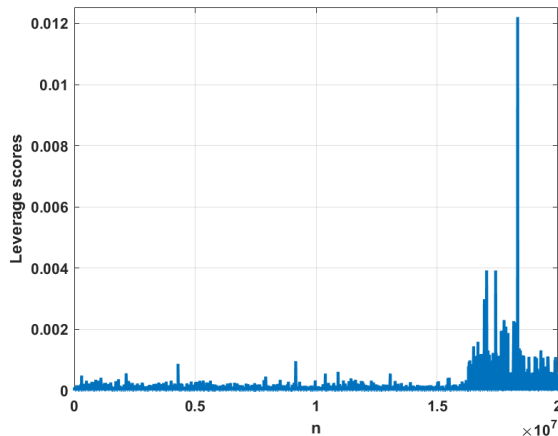
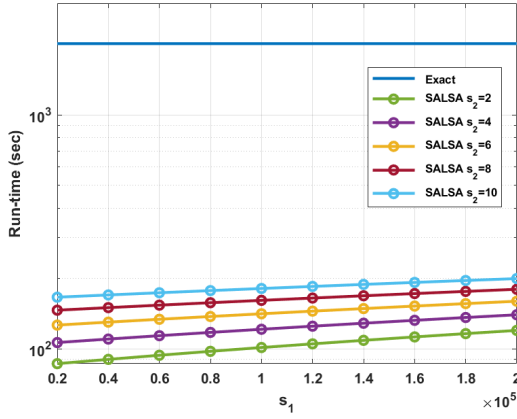


Figure 3

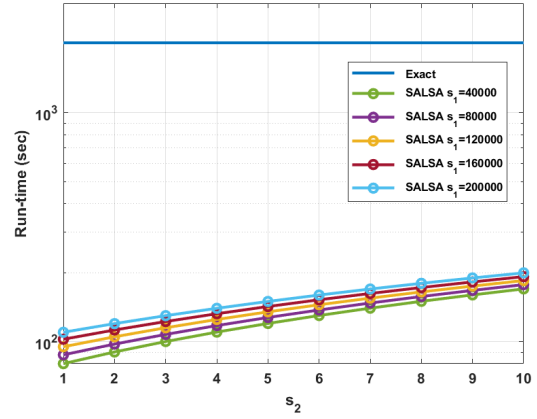
Figure 4: Non-uniform distribution of leverage-scores of the real-data matrix with $m = 20,000,000$ rows and $n = 160$ columns extracted from weight data of a huge knowledge graph in [49].

computed only once, because the exact algorithm does not have any stochastic components. However, when estimating the leverage-scores using **SALSA**, we perform calculations for every combination of (s_1, s_2) , where $s_1 \in \{20,000, 40,000, \dots, 200,000\}$ and $s_2 \in \{1, 2, \dots, 10\}$. We repeated this process 50 times to remove the impact of potential fluctuations. Figure 5 provides details on execution times and MAPE for both the exact algorithm and **SALSA** for each (s_1, s_2) pair.

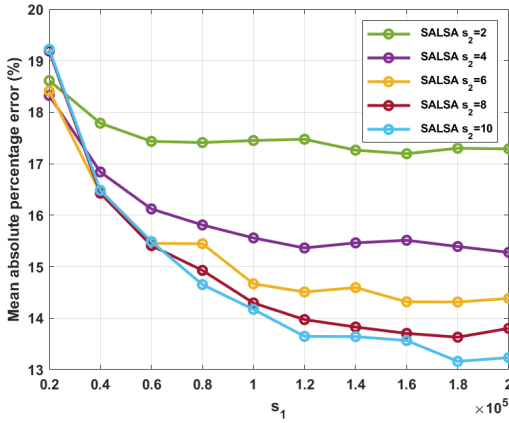
Figures 5a and 5b illustrate the efficiency of **SALSA** in estimating leverage-scores based on the values of s_1 and s_2 when compared with the exact algorithm. Evidently, as s_1 or s_2 increases, **SALSA** needs to handle a larger sketch of the original data matrix, subsequently requiring more time for leverage-score estimation. This consistent linear trend remains noticeable regardless of variations in either s_1 or s_2 . Furthermore, these plots highlight that variations in s_2 have a greater impact than increases in s_1 . The gaps between the curves representing different levels of s_2 in Figures 5a are significantly larger than the differences between the curves for varying levels of s_1 in Figure 5b. This observation aligns with the innovation introduced in **SALSA**, which employs column-wise sketching with s_2 to enhance the



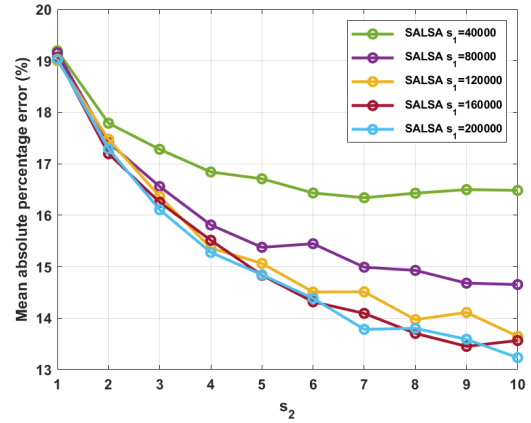
(a)



(b)



(c)



(d)

Figure 5: (5a) shows the run times of approximating leverage-scores of the real-data matrix as a function of s_2 for different values of s_1 , while (5b) displays the run times as a function of s_2 for different fixed values of s_1 . Run time for using the exact method in computing the leverage-scores is depicted in blue. The real-data matrix contains $m = 20,000,000$ rows and $n = 160$ columns, extracted from the edge-weight data matrix in [49]. Furthermore, (5c) presents the MAPE against s_1 , and (5d) depicts the same error metric against s_2 between the exact and estimated leverage-scores.

numerical performance of estimating leverage-scores. Whereas exact leverage-score computation takes 2,017 seconds (approximately 33 minutes) for the whole data matrix, the most time-demanding pair, $s_1 = 200,000$ and $s_2 = 10$, requires only 3.3 minutes. This finding indicates an approximately 10-fold increase in execution efficiency. The least time-demanding pair, $s_1 = 20,000$ and $s_2 = 1$, only requires about one minute for leverage-score estimation.

Figures 5c and 5d explain the reduction in the percentage error when estimating leverage-scores as functions of s_1 and s_2 . MAPE, defined in (18), measures the MAPE between the

estimated leverage-scores and those computed exactly. As both s_1 and s_2 increase, the approximate matrix incorporates more information from the original matrix, leading to more accurate leverage-score estimations. For instance, when s_1 and s_2 hit their highest values, namely, $s_2 = 10$ or $s_1 = 200,000$, the lowest error curves are observed. The highest error of 19.69% occurred when $s_1 = 20,000$ and $s_2 = 10$, whereas the lowest MAPE of 13.16% occurred for $s_1 = 180,000$ and $s_2 = 10$. With a worst-case MAPE of approximately 20% and a 5-fold reduction in execution time, these results signify the efficiency of SALSA in estimating leverage-scores.

Another interesting observation about SALSA when applied to real-data matrices, as depicted in Figure 5c, is that increasing the value of s_1 while keeping s_2 fixed does not appear to lead to significant improvements in the mean-absolute-error levels. However, Figure 5d reveals that by increasing the value of s_2 while holding s_1 constant, achieving a reduction in the MAPE.

5 LSARMA: Application of SALSA in Big Time Series Data

This section demonstrates an application of the theory established in Section 3 regarding approximating leverage-scores. We employ SALSA in the development of a novel algorithm designed for fitting autoregressive moving average (ARMA) models in scenarios involving big data. To provide context, we begin with a concise overview of the necessary background information on ARMA models and the MLE of their parameters.

5.1 ARMA Models

A time series $\{X_t; t = 0, \pm 1, \pm 2, \dots\}$ is a sequence of random variables indexed according to the order they are observed in time. The main goal of time series analysis is to create statistical models that predict the future behavior of a system. These models have established their efficacy and benefits in the modeling and analysis of stochastic dynamic systems. Their popularity is increasing for a variety of applications, ranging from supply chains and energy systems to epidemiology and engineering problems [1, 20, 21, 26].

Each observed value of X_t is labeled x_t . A time series X_t is considered (weakly) stationary if its mean function $\mathbb{E}[X_t]$ is constant, and the autocovariance function $Cov(X_t, X_{t+h})$ is independent of time.

ARMA models are a class of statistical models designed for the analysis and forecasting of stationary time series data. These models are characterized by their order, denoted as $\text{ARMA}(p, q)$, which specifies the order of the autoregressive component (p) and the moving average component (q). In practice, a specific ARMA model is fully identified by estimating the parameters $\phi = (\phi_1, \dots, \phi_p)$ and $\theta = (\theta_1, \dots, \theta_q)$, as illustrated in

$$X_t = \phi_1 X_{t-1} + \dots + \phi_p X_{t-p} + \theta_1 W_{t-1} + \dots + \theta_q W_{t-q} + W_t,$$

where $\phi_p \neq 0$ and $\theta_q \neq 0$. Additionally, $\{W_t; t = 0, \pm 1, \pm 2, \dots\}$ is a Gaussian white noise process with the properties $\mathbb{E}[W_t] = 0$ and $Cov(W_t, W_s) = \delta_{ts} \sigma_W^2$, where δ_{ts} denotes the

Kronecker delta. Note we can assume $\mathbb{E}[X_t] = 0$ without any loss of generality. If $\mathbb{E}[X_t] = \mu \neq 0$, a simple transformation can be applied by replacing X_t with $Y_t = X_t - \mu$ to hold this assumption. Furthermore, an $\text{ARMA}(p, q)$ process is said to be invertible if the time series can be written as

$$W_t = \sum_{j=0}^{\infty} \pi_j X_{t-j}, \quad \text{where } \pi_0 = 1 \text{ and } \sum_{j=0}^{\infty} |\pi_j| < \infty. \quad (19)$$

Equivalently, the process is considered invertible if and only if the roots of the MA polynomial $\Theta_q(z) = 1 + \theta_1 z + \dots + \theta_q z^q$, for $z \in \mathbb{C}$, lie outside the unit circle. We assume all subsequent ARMA processes are causal, invertible, and stationary unless explicitly stated otherwise.

A total of $p + q + 3$ parameters need to be estimated when fitting an ARMA model, which includes the orders p and q , coefficients ϕ_i and θ_i , and the variance of the white noise σ_W^2 . The estimation of the orders p and q requires the analysis of the Autocorrelation Function (ACF) and Partial Autocorrelation Function (PACF) plots. These functions help identify the number of past observations that significantly influence the current value in the time series (see [47] for details). The estimation of coefficients ϕ_i , θ_i , and σ_W^2 through the maximum likelihood technique is discussed in the next section.

5.2 Maximum Likelihood Estimation of the Parameters

Consider a time series realization x_1, \dots, x_n generated by an $\text{ARMA}(p, q)$ process, where the orders p and q are known and the length of the series n is significantly larger than p and q . This section considers the estimation of the parameters $\phi_1, \dots, \phi_p, \theta_1, \dots, \theta_q$, and σ_W^2 through the MLE method. Obtaining an analytical expression for the estimates is intractable due to the complicated and nonlinear nature of the log-likelihood function, which is defined as

$$\log(f_{X_1, \dots, X_n}(x_1, \dots, x_n; \phi_1, \dots, \phi_p, \theta_1, \dots, \theta_q, \sigma_W^2)),$$

where f is the joint probability distribution function of the random variables X_1, \dots, X_n . As a result, numerical optimization techniques are typically used to approximate these estimates. These techniques explore parameter values that maximize the log-likelihood function so that the model fits the observed data as accurately as possible. However, we can demonstrate that the conditional log-likelihood function, described below, shares similarities with the log-likelihood function of a linear regression model:

$$\begin{aligned} & \log(f_{X_{p+1}, \dots, X_n | X_1, \dots, X_p, W_1, \dots, W_q}(x_{p+1}, \dots, x_n; \phi_1, \dots, \phi_p, \theta_1, \dots, \theta_q, \sigma_W^2 | x_1, \dots, x_p, w_1, \dots, w_q)) \\ &= -\frac{n-p}{2} \log(2\pi) - \frac{n-p}{2} \log(\sigma_W^2) \\ & \quad - \sum_{t=p+1}^n \frac{(x_t - \phi_1 x_{t-1} - \dots - \phi_p x_{t-p} - \theta_1 w_{t-1} - \dots - \theta_q w_{t-q})^2}{2\sigma_W^2}, \end{aligned}$$

where the log-likelihood has been conditioned on the first p observations, equivalent to the order of the AR component, and the first q white noises, equivalent to the order of the MA component [29]. This similarity allows for the use of regression-based optimization techniques

in estimating the parameters of an ARMA model. Hence, the conditional MLE (CMLE) of the coefficients and the variance can be obtained through an OLS regression of x_t against its own lagged values up to order p and the previous white noise terms up to order q . However, in practice, the previous white noise terms are not directly available and must be estimated from the available data before this approach can be applied.

J. Durbin's method [19], which was originally developed for fitting MA models, has been extended to handle ARMA processes. The approach involves fitting an AR model to the data and then using the residuals of this model to estimate the parameters of the MA model. We refer to this method as Durbin's algorithm here. Durbin's algorithm allows for the estimation of the unobserved white noise terms, hence enabling the OLS approach to be used when the noise terms are unavailable. Equation (19) shows any invertible ARMA(p, q) process can be equivalently represented as an AR(∞) process. However, in practice, due to finite sample sizes, Durbin's algorithm first fits an AR model with a sufficiently large order, denoted as \tilde{p} (where $\tilde{p} \ll n$), to the data. Next, the algorithm approximates the values of the white noise term W_t by computing the residuals of the fitted AR model,

$$\hat{w}_t = x_t - \sum_{j=1}^{\tilde{p}} \hat{\pi}_j x_{t-j}. \quad (20)$$

Subsequently, as the next step, the algorithm approximates the CMLE of the coefficient vector $\boldsymbol{\psi}_{n,p,q} = (\phi_1, \dots, \phi_p, \theta_1, \dots, \theta_q)^\top$ as

$$\hat{\boldsymbol{\psi}}_{n,p,q} = (\mathbf{X}_{n,p,q}^\top \mathbf{X}_{n,p,q})^{-1} \mathbf{X}_{n,p,q}^\top \mathbf{x}_{n,p,q}, \quad (21)$$

where the data matrix $\mathbf{X}_{n,p,q}$ is defined as

$$\begin{pmatrix} x_{q+\tilde{p}} & \cdots & x_{q+\tilde{p}-p+1} & \hat{w}_{q+\tilde{p}} & \cdots & \hat{w}_{\tilde{p}+1} \\ x_{q+\tilde{p}+1} & \cdots & x_{q+\tilde{p}-p+2} & \hat{w}_{q+\tilde{p}+1} & \cdots & \hat{w}_{\tilde{p}+2} \\ \vdots & \ddots & \vdots & \vdots & \ddots & \vdots \\ x_{n-1} & \cdots & x_{n-p} & \hat{w}_{n-1} & \cdots & \hat{w}_{n-q} \end{pmatrix}, \quad (22)$$

and $\mathbf{x}_{n,p,q} := (x_{q+\tilde{p}+1}, x_{q+\tilde{p}+2}, \dots, x_n)^\top$. Moreover, the CMLE of σ_W^2 is obtained by

$$\hat{\sigma}_W^2 = \frac{\|\hat{\mathbf{r}}_{n,p,q}\|^2}{(n-p-q)},$$

where $\hat{\mathbf{r}}_{n,p,q} := \mathbf{X}_{n,p,q} \hat{\boldsymbol{\psi}}_{n,p,q} - \mathbf{x}_{n,p,q}$ is the residual vector. Hannan and Rissanen [30] extended this algorithm with an additional set of trimming steps to improve the initial parameter estimates.

5.3 Choosing a Sufficiently Large \tilde{p}

The equivalence between invertible $\text{ARMA}(q)$ and $\text{AR}(\infty)$ models might imply larger values of \tilde{p} would consistently outperform smaller ones. However, this equivalence does not consider finite sample sizes. As noted in [4],

Practice and simulations have shown that the best AR order in estimation is finite and depends on the true process parameters and the number of observations.

Since the first procedure in estimating \tilde{p} in [19], various methods have been developed to select the most suitable value.

As an example, Hannan and Rissanen [30] proposed the use of the Bayesian information criterion (BIC) to determine the optimal value of \tilde{p} . This criterion can be applied to a regression model with k coefficients. In this context, the MLE for the variance is denoted as $\hat{\sigma}_k^2 = \text{SSE}(k)/n$, where $\text{SSE}(k)$ represents the residual sum of squares under the model with k regression coefficients. Then,

$$\text{BIC} := \log(\hat{\sigma}_k^2) + \frac{k \log(n)}{n}, \quad (23)$$

with the value of k yielding the minimum BIC specifying the best regression model. Additionally, Broersen [4] recommended selecting the optimal order as the one that minimizes the $\text{GIC}(p, 1)$ criterion, where p ranges from zero to infinity. Here, GIC stands for a generalization of Akaike's information criterion, offering a practical approach to determining the most suitable order for AR models. More recently, the rolling average algorithm, introduced by Eshragh et al. [22], is a method for selecting an optimal \tilde{p} when fitting ARMA models, especially in the context of big time series datasets.

5.4 The LSARMA Algorithm

We now introduce LSARMA, as presented in Algorithm 2. This algorithm is based on the theoretical foundations outlined in Section 3 and extends the LSAR algorithm [24]. LSAR uses leverage-score sampling and the Toeplitz structure of the data matrix to approximate AR models for large time series datasets, and LSARMA offers a generalization to ARMA models.

Remark 1 (LSARMA Computational Complexity, [24], Theorem 6). The computational bottleneck of the LSARMA algorithm is due to the use of the LSAR algorithm. Consequently, the worst-case time complexity of the LSARMA algorithm is the same as that of the LSAR algorithm, that is,

$$\mathcal{O} \left(n\tilde{p} + \frac{\tilde{p}^4 \log \tilde{p}}{\varepsilon_1^2} \right),$$

where ε_1 is introduced in Theorem 2. Note exact $\text{ARMA}(p, q)$ fitting requires $\mathcal{O}(n\tilde{p}^3)$.

Algorithm 2 LSARMA

Input: Time series data $\{x_1, \dots, x_n\}$, relatively large order $\bar{p} \ll n$, an estimate of the MA order q ;

Apply the LSAR algorithm using the *BIC* criterion, as in (23), to choose a suitable \tilde{p} to obtain the white noise estimates \hat{w}_t as in (20);

Construct the data matrix $\mathbf{X}_{n,0,q}$ as in (22) and estimate its leverage-scores using SALSAs;
for $h = 1$ **to** \bar{p} **do**

 Use SALSAs to estimate the leverage-scores of $\mathbf{X}_{n,h,q}$;

 Use the estimated leverage-scores to find the counterpart sketched solution as given in (14), of $\hat{\psi}_{n,h,q}$ as in (21)

 Compute the PACF_h

end for

Plot PACF_h against h to estimate the AR order p .

Output: Estimated orders p , q and parameter vector $\hat{\psi}_{n,p,q}$.

5.5 Numerical Results: Big Time Series Data

The numerical results comparing the execution time and percentage error of parameter estimation using LSARMA versus an exact method for synthetic $\text{MA}(q)$ data with $n = 5,000,000$ entries are illustrated in Figure 6. Although the exact method is executed only once, because it lacks any randomization in its procedure, the LSARMA method is run for 25 iterations due to the inclusion of a stochastic sketching module within its procedure. Consequently, the results of LSARMA are averaged to facilitate a meaningful comparison with the exact method.

The benefits of employing LSARMA for estimating the model parameters are evident in Figure 6a. As the value of q increases, both methods show positive slopes in their computational time curves, but LSARMA consistently requires significantly fewer resources. To grasp the computational advantage, note the average execution time for the exact method remains at 106,875 seconds (about 30 hours) for all values of q , whereas LSARMA averages at only 3,526 seconds (about one hour), making it approximately 30 times faster. Furthermore, when considering all values of q , the maximum time required for the exact method to find the parameters is a substantial 89 hours, whereas LSARMA accomplishes the task in a mere 3 hours.

These results presented in Figure 6a underscore the superior performance and efficiency of LSARMA over the exact method, particularly as the complexity of the data increases. This advantage becomes even more significant as the value of q grows, highlighting the practicality, scalability, and computational gain of using LSARMA for parameter estimation in $\text{MA}(q)$ data.

To further demonstrate the efficiency of LSARMA, we visualize its computational accuracy in comparison to the exact method by analyzing the percentage error between the parameters obtained from both methods in Figure 6b. To calculate the percentage error for each value

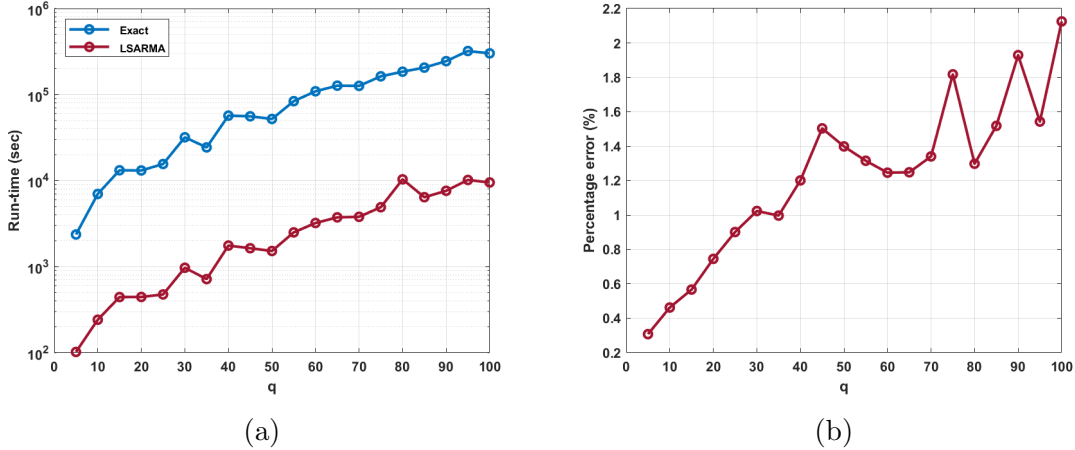


Figure 6: (6a) Run times in computing exact and estimated parameters and (6b) percentage error in the difference between exact and estimated parameters for synthetic $MA(q)$ data with $n = 5,000,000$ entries.

of q , we use the Euclidean norm as follows:

$$\text{Percentage error} = \frac{\|\psi_{n,p,q} - \hat{\psi}_{n,p,q}\|}{\|\psi_{n,p,q}\|} \times 100\%. \quad (24)$$

Although a slight upward trend occurs in the percentage error as q increases, it remains remarkably low, with the maximum percentage error across all values of q being only 2.1%. This outstanding result showcases the accuracy of parameter estimation in large time series data using LSARMA, even when working with just a fraction of the data. Occasional fluctuations are observed for q values greater than 75. We attribute these fluctuations primarily to the resource allocation of MATLAB. However, these fluctuations are minimal - less than 0.2% - and can be considered negligible given the data size.

Considering both its computational efficiency and accuracy over the exact method in Figure 6, LSARMA represents itself as a reliable and robust method for estimating parameters in MA models. With a significant reduction in execution time, approximately 30 times faster than the exact method, and only a marginal deviation of 2.1% from the parameters obtained from the exact method, LSARMA proves to be an excellent choice for parameter estimation in large time series data.

Furthermore, the LSARMA algorithm finds application in estimating parameters for synthetically generated $ARMA(p, q)$ models, with p and q selected from the set $\{5, 10, 20, 40, 80\}$, and data models containing $n = 5,000,000$ entries. These datasets are constructed with randomly generated data; hence, they contain varying levels of complexity in parameter estimation, due to the differing characteristics of the underlying models. For each specific model, the true parameters are determined exactly only once, because no stochasticity is involved in this process. Subsequently, the LSARMA algorithm is employed to estimate these parameters, and this estimation process is repeated ten times to account for variability.

Both the execution time and the percentage of errors, as defined in (24), are computed for each method. The results of these experiments are visually presented in Figure 7, providing insights into the algorithm's performance across a range of $\text{ARMA}(p, q)$ models with distinct complexities.

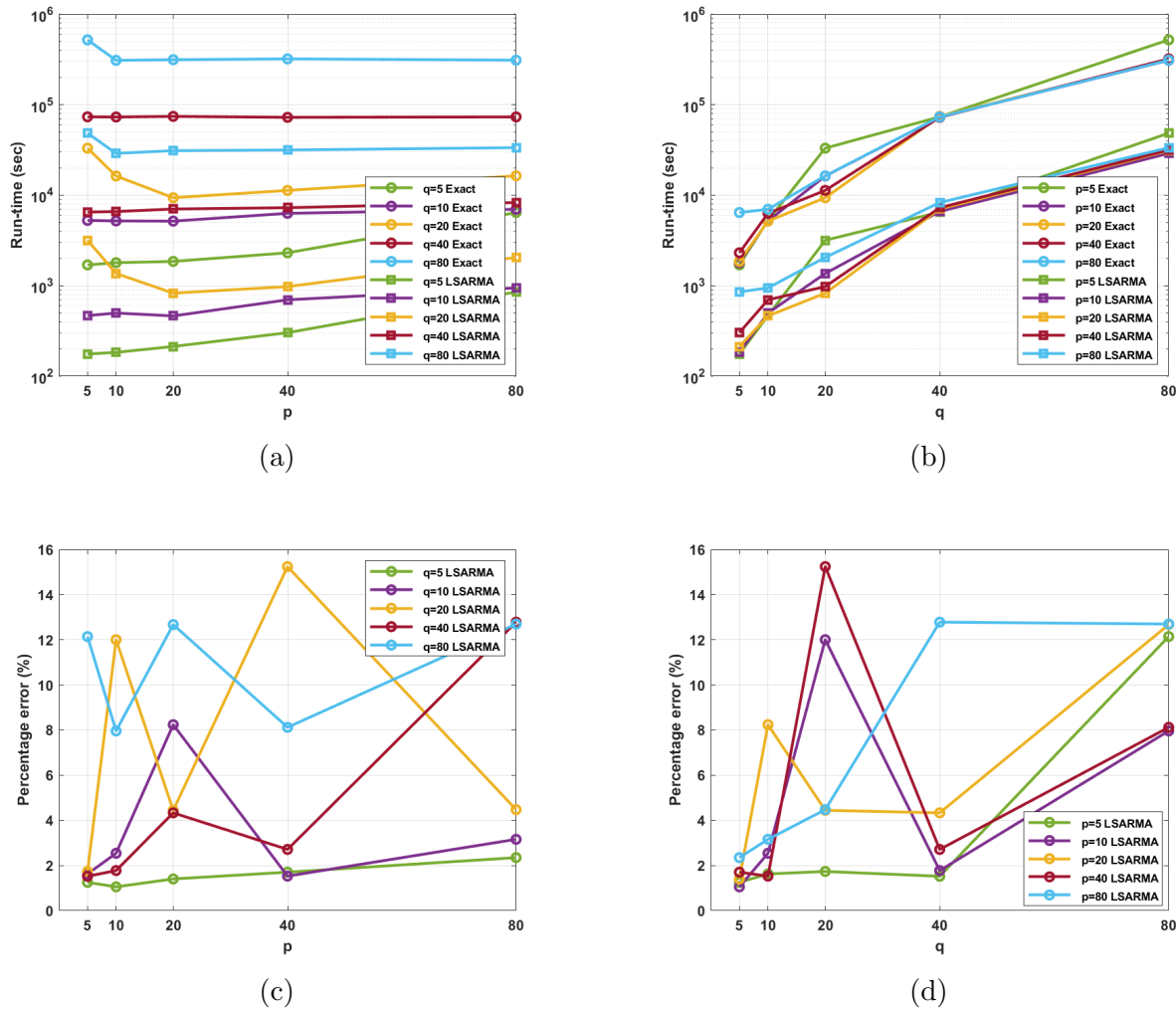


Figure 7: (7a) shows the run times as functions of p for different values of q for computing both exact and estimated parameters, while (7b) displays the run times as functions of q for different fixed values of p . These results are obtained for synthetic $\text{ARMA}(p, q)$ models with $p, q \in \{5, 10, 20, 40, 80\}$ and $n = 5,000,000$ entries. Furthermore, (7c) presents the MAPE against p , and (7d) depicts the same error metric against q between the exact and LSARMA algorithms.

From a time-efficiency perspective, Figures 7a and 7b provide a comprehensive illustration of the computational time required to obtain exact and estimated parameters using the exact and LSARMA algorithms, respectively. These figures present insights into how this

computational time changes across different combinations of p and q values. In both scenarios, note the most time-intensive computations are associated with the $\text{ARMA}(5, 80)$ model. Specifically, the exact algorithm demands 521,132 seconds (approximately 145 hours) to complete, whereas the LSARMA algorithm accomplishes the same task in significantly less time, taking only 48,495 seconds (roughly 13 hours). This remarkable efficiency is evidenced by the fact that, for the most computationally demanding model, LSARMA is approximately 11 times faster than the exact algorithm. Conversely, the least computationally demanding model, $\text{ARMA}(5, 5)$, can be estimated in 47 minutes using the exact algorithm and only 3 minutes with the LSARMA algorithm. Here, LSARMA shows approximately a 16-times increase in efficiency.

Additionally, Figures 7a and 7b provide insights into execution times by fixing values of either q or p while varying the other variable. Particularly, Figure 7a demonstrates nearly constant execution times when q is fixed and p values are varied. Conversely, Figure 7b reveals an increasing trend in execution times when p is held constant, and q values are changed. These observations shed light on the complicated interplay between p and q in determining the computational time required for parameter estimation. Note the execution time of the exact algorithm and LSARMA share the same color, but different markers of \circ and \square , respectively.

Figures 7c and 7d provide graphical representations of the percentage error between parameters estimated by the exact and LSARMA algorithms, as defined in (24). Given the random construction of models for each combination of (p, q) , these models inherently possess varying degrees of complexity, resulting in fluctuating error curves as p or q change. Consequently, the observed fluctuations in the error curves can be attributed to these inherent variations. Particularly, the maximum percentage error, amounting to 15.24%, is observed in parameter estimation for the $\text{ARMA}(40, 20)$ model. Conversely, the minimum percentage error, at only 1.05%, is observed for the $\text{ARMA}(10, 5)$ model. On average, across all models considered, the percentage error in parameter estimation between the exact and LSARMA algorithms is approximately 4.63%, with a standard deviation of 5.58%.

These statistics offer valuable insights into the overall accuracy and consistency of parameter estimation achieved by the LSARMA algorithm, when compared with the exact method. With an average percentage error of just 4.63%, coupled with the significant efficiency gains of being approximately 11 times faster in terms of execution time, the LSARMA algorithm clearly demonstrates its superior capability in reliably estimating the parameters of $\text{ARMA}(p, q)$ models.

A Technical Lemmas and Proofs

A.1 Proof of Theorem 1 (Exact Recursive Leverage Scores)

We first present Lemma 1, which we use in the proof of Theorem 1.

Lemma 1 (Block Matrix Inversion Lemma [28]). *Consider the 2×2 block matrix*

$$\mathbf{M} = \begin{bmatrix} \mathbf{A}_{m,d} & \mathbf{b} \\ \mathbf{b}^\top & c \end{bmatrix},$$

where $\mathbf{A}_{m,d} \in \mathbb{R}^{m \times d}$, $\mathbf{b} \in \mathbb{R}^{m \times 1}$ and $c \in \mathbb{R}$. If $\mathbf{A}_{m,d}$ is invertible, the inverse of \mathbf{M} exists and can be calculated as follows:

$$\mathbf{M}^{-1} = \frac{1}{k} \begin{bmatrix} k\mathbf{A}_{m,d}^{-1} + \mathbf{A}_{m,d}^{-1}\mathbf{b}\mathbf{b}^\top\mathbf{A}_{m,d}^{-1} & -\mathbf{A}_{m,d}^{-1}\mathbf{b} \\ -\mathbf{b}^\top\mathbf{A}_{m,d}^{-1} & 1 \end{bmatrix},$$

where $k = c - \mathbf{b}^\top\mathbf{A}_{m,d}^{-1}\mathbf{b}$.

Proof of Theorem 1

Proof. The i^{th} leverage score of $\mathbf{A}_{m,d}$ is given by the i^{th} diagonal element of the hat matrix $\mathbf{H}_{m,d}$, that is,

$$\ell_{m,d}(i) = \mathbf{H}_{m,d}(i, i) = \left[\mathbf{A}_{m,d} \left(\mathbf{A}_{m,d}^\top \mathbf{A}_{m,d} \right)^{-1} \mathbf{A}_{m,d}^\top \right] (i, i).$$

Now consider $\left(\mathbf{A}_{m,d}^\top \mathbf{A}_{m,d} \right)^{-1}$, where

$$\mathbf{A}_{m,d}^\top \mathbf{A}_{m,d} = \begin{bmatrix} \mathbf{A}_{m,d-1}^\top \\ \mathbf{a}_{d-1}^\top \end{bmatrix} \begin{bmatrix} \mathbf{A}_{m,d-1} & \mathbf{a}_{d-1} \end{bmatrix} = \begin{bmatrix} \mathbf{A}_{m,d-1}^\top \mathbf{A}_{m,d-1} & \mathbf{A}_{m,d-1}^\top \mathbf{a}_{d-1} \\ \mathbf{a}_{d-1}^\top \mathbf{A}_{m,d-1} & \mathbf{a}_{d-1}^\top \mathbf{a}_{d-1} \end{bmatrix}.$$

Using the notation from Lemma 1, we have

$$\begin{aligned} k &= \mathbf{a}_{d-1}^\top \mathbf{a}_{d-1} - \mathbf{a}_{d-1}^\top \mathbf{A}_{m,d-1} \left(\mathbf{A}_{m,d-1}^\top \mathbf{A}_{m,d-1} \right)^{-1} \mathbf{A}_{m,d-1}^\top \mathbf{a}_{d-1} \\ &= \mathbf{a}_{d-1}^\top \left(\mathbf{a}_{d-1} - \mathbf{A}_{m,d-1} \boldsymbol{\phi}_{m,d-1} \right) \\ &= -\mathbf{a}_{d-1}^\top \mathbf{r}_{m,d-1}. \end{aligned}$$

Hence,

$$\left(\mathbf{A}_{m,d}^\top \mathbf{A}_{m,d} \right)^{-1} = \frac{-1}{\mathbf{a}_{d-1}^\top \mathbf{r}_{m,d-1}} \begin{bmatrix} -\mathbf{a}_{d-1}^\top \mathbf{r}_{m,d-1} \left(\mathbf{A}_{m,d-1}^\top \mathbf{A}_{m,d-1} \right)^{-1} + \boldsymbol{\phi}_{m,d-1} \boldsymbol{\phi}_{m,d-1}^\top & -\boldsymbol{\phi}_{m,d-1} \\ -\boldsymbol{\phi}_{m,d-1}^\top & 1 \end{bmatrix}.$$

Restricting attention to the i^{th} diagonal element, we have

$$\ell_{m,d}(i) = \mathbf{A}_{m,d}(i, :) \left(\mathbf{A}_{m,d}^\top \mathbf{A}_{m,d} \right)^{-1} \mathbf{A}_{m,d}^\top(:, i)$$

$$\begin{aligned}
&= \frac{-1}{\mathbf{a}_{d-1}^\top \mathbf{r}_{m,d-1}} \begin{pmatrix} \mathbf{A}_{m,d-1}(i, :) & \mathbf{a}_{d-1}(i) \end{pmatrix} \\
&\quad \times \begin{bmatrix} -\mathbf{a}_{d-1}^\top \mathbf{r}_{m,d-1} (\mathbf{A}_{m,d-1}^\top \mathbf{A}_{m,d-1})^{-1} + \phi_{m,d-1} \phi_{m,d-1}^\top & -\phi_{m,d-1} \\ -\phi_{m,d-1}^\top & 1 \end{bmatrix} \begin{pmatrix} \mathbf{A}_{m,d-1}^\top(:, i) \\ \mathbf{a}_{d-1}(i) \end{pmatrix} \\
&= \frac{-1}{\mathbf{a}_{d-1}^\top \mathbf{r}_{m,d-1}} \begin{pmatrix} -\mathbf{a}_{d-1}^\top \mathbf{r}_{m,d-1} \mathbf{A}_{m,d-1}(i, :) (\mathbf{A}_{m,d-1}^\top \mathbf{A}_{m,d-1})^{-1} \\ + \mathbf{A}_{m,d-1}(i, :) \phi_{m,d-1} \phi_{m,d-1}^\top - \mathbf{a}_{d-1}(i) \phi_{m,d-1}^\top \\ -\mathbf{A}_{m,d-1}(i, :) \phi_{m,d-1} + \mathbf{a}_{d-1}(i) \end{pmatrix}^\top \\
&\quad \times \begin{pmatrix} \mathbf{A}_{m,d-1}^\top(:, i) \\ \mathbf{a}_{d-1}(i) \end{pmatrix} \\
&= \frac{-1}{\mathbf{a}_{d-1}^\top \mathbf{r}_{m,d-1}} \begin{pmatrix} -\mathbf{a}_{d-1}^\top \mathbf{r}_{m,d-1} \mathbf{A}_{m,d-1}(i, :) (\mathbf{A}_{m,d-1}^\top \mathbf{A}_{m,d-1})^{-1} \mathbf{A}_{m,d-1}^\top(:, i) \\ + \mathbf{A}_{m,d-1}(i, :) \phi_{m,d-1} \phi_{m,d-1}^\top \mathbf{A}_{m,d-1}^\top(:, i) - \mathbf{a}_{d-1}(i) \phi_{m,d-1}^\top \mathbf{A}_{m,d-1}^\top(:, i) \\ - \mathbf{A}_{m,d-1}(i, :) \phi_{m,d-1} \mathbf{a}_{d-1}(i) + \mathbf{a}_{d-1}(i)^2 \end{pmatrix}. \tag{25}
\end{aligned}$$

Note we have

$$\begin{aligned}
\mathbf{a}_{d-1}^\top \mathbf{r}_{m,d-1} &= (\mathbf{A}_{m,d-1} \phi_{m,d-1} - \mathbf{r}_{m,d-1})^\top \mathbf{r}_{m,d-1} \\
&= \phi_{m,d-1}^\top \mathbf{A}_{m,d-1}^\top \mathbf{r}_{m,d-1} - \mathbf{r}_{m,d-1}^\top \mathbf{r}_{m,d-1} \\
&= -\|\mathbf{r}_{m,d-1}\|^2, \tag{26}
\end{aligned}$$

as by (12) and the normal equations $\mathbf{A}_{m,d-1}^\top \mathbf{A}_{m,d-1} \phi_{m,d-1} = \mathbf{A}_{m,d-1}^\top \mathbf{a}_{d-1}$. Equations (25) and (26) imply

$$\begin{aligned}
\ell_{m,d}(i) &= \ell_{m,d-1}(i) + \frac{1}{\|\mathbf{r}_{m,d-1}\|^2} \left((\mathbf{r}_{m,d-1}(i) + \mathbf{a}_{d-1}(i))^2 \right. \\
&\quad \left. - 2\mathbf{a}_{d-1}(i) (\mathbf{r}_{m,d-1}(i) + \mathbf{a}_{d-1}(i)) + \mathbf{a}_{d-1}(i)^2 \right) \\
&= \ell_{m,d-1}(i) + \frac{(\mathbf{r}_{m,d-1}(i))^2}{\|\mathbf{r}_{m,d-1}\|^2}.
\end{aligned}$$

□

A.2 Proof of Theorem 4 (Relative Errors for Approximate Leverage-Scores)

To prove Theorem 4, we first introduce Lemmas 2–8.

Lemma 2. The i^{th} leverage score of a matrix $\mathbf{A}_{m,d} \in \mathbb{R}^{m \times d}$ is given by

$$\ell_{m,d}(i) = \min_{\mathbf{z} \in \mathbb{R}^m} \{ \|\mathbf{z}\|^2 \text{ s.t. } \mathbf{A}_{m,d}^\top \mathbf{z} = \mathbf{A}_{m,d}(i, :) \},$$

for $i = 1, \dots, m$.

Proof. The Lagrangian function for the minimization problem is defined as

$$h(\mathbf{z}, \boldsymbol{\lambda}) := \frac{1}{2} \mathbf{z}^\top \mathbf{z} - \boldsymbol{\lambda}^\top (\mathbf{A}_{m,d}^\top \mathbf{z} - \mathbf{A}_{m,d}(i, :)).$$

Because the objective function and the linear constraints are convex, by taking the first derivative with respect to the vector \mathbf{z} and setting equal to zero, we have

$$\frac{\partial h(\mathbf{z}, \boldsymbol{\lambda})}{\partial \mathbf{z}} = \mathbf{z} - \mathbf{A}_{m,d} \boldsymbol{\lambda} = 0 \implies \mathbf{z}^* = \mathbf{A}_{m,d} \boldsymbol{\lambda}^*.$$

By multiplying both sides of this expression by $\mathbf{A}_{m,d}^\top$, we obtain

$$\mathbf{A}_{m,d}^\top \mathbf{z}^* = \mathbf{A}_{m,d}^\top \mathbf{A}_{m,d} \boldsymbol{\lambda}^*,$$

which is equivalent to

$$\mathbf{A}_{m,d}(i, :) = \mathbf{A}_{m,d}^\top \mathbf{A}_{m,d} \boldsymbol{\lambda}^*,$$

implying

$$\boldsymbol{\lambda}^* = (\mathbf{A}_{m,d}^\top \mathbf{A}_{m,d})^{-1} \mathbf{A}_{m,d}(i, :).$$

Thus,

$$\mathbf{z}^* = \mathbf{A}_{m,d} (\mathbf{A}_{m,d}^\top \mathbf{A}_{m,d})^{-1} \mathbf{A}_{m,d}(i, :).$$

Finally, we have

$$\begin{aligned} \|\mathbf{z}^*\|^2 &= (\mathbf{z}^*)^\top (\mathbf{z}^*) \\ &= (\mathbf{A}_{m,d}^\top (i, :) (\mathbf{A}_{m,d}^\top \mathbf{A}_{m,d})^{-1} \mathbf{A}_{m,d}^\top) (\mathbf{A}_{m,d} (\mathbf{A}_{m,d}^\top \mathbf{A}_{m,d})^{-1} \mathbf{A}_{m,d}(i, :)) \\ &= \mathbf{A}_{m,d}^\top (i, :) (\mathbf{A}_{m,d}^\top \mathbf{A}_{m,d})^{-1} \mathbf{A}_{m,d}(i, :) \\ &= \ell_{m,d}(i). \end{aligned}$$

□

Lemma 3. For $\mathbf{A}_{m,d} \in \mathbb{R}^{m \times d}$, we have

$$\|\mathbf{A}_{m,d}(i, :)\| \leq \|\mathbf{A}_{m,d}\| \sqrt{\ell_{m,d}(i)}, \quad \text{for } i = 1, \dots, m.$$

Proof. From the minimisation constraints in Lemma 2, we have

$$\begin{aligned}\|\mathbf{A}_{m,d}(i, :)\| &= \|\mathbf{A}_{m,d}^\top \mathbf{z}^*\| \\ &\leq \|\mathbf{A}_{m,d}^\top\| \|\mathbf{z}^*\| \\ &= \|\mathbf{A}_{m,d}\| \sqrt{\ell_{m,d}(i)}.\end{aligned}$$

□

Lemma 4. For $\mathbf{A}_{m,d} \in \mathbb{R}^{m \times d}$ and $i = 1, \dots, m$, we have

$$|\mathbf{r}_{m,d-1}(i)| \leq \sqrt{\|\boldsymbol{\phi}_{m,d-1}\|^2 + 1} \|\mathbf{A}_{m,d}\| \sqrt{\ell_{m,d}(i)}, \quad (27a)$$

$$|\hat{\mathbf{r}}_{m,d-1}(i)| \leq \sqrt{\|\hat{\boldsymbol{\phi}}_{m,d-1}\|^2 + 1} \|\mathbf{A}_{m,d}\| \sqrt{\ell_{m,d}(i)}, \quad (27b)$$

$$|\hat{\hat{\mathbf{r}}}_{m,d-1}(i)| \leq (1 + \varepsilon_2) \sqrt{\|\hat{\boldsymbol{\phi}}_{m,d-1}\|^2 + 1} \|\mathbf{A}_{m,d}\| \sqrt{\ell_{m,d}(i)} \quad (27c)$$

where ε_2 , $\mathbf{r}_{m,d}$, $\hat{\mathbf{r}}_{m,d}$, $\hat{\hat{\mathbf{r}}}_{m,d}$, $\boldsymbol{\phi}_{m,d}$, $\hat{\boldsymbol{\phi}}_{m,d}$ and $\hat{\hat{\boldsymbol{\phi}}}_{m,d}$ are defined respectively in Theorem 3, (12), (15), (16), (11), (14) and (17).

Proof. By Lemma 3, the right-hand side of (27a) can be found as follows:

$$\begin{aligned}|\mathbf{r}_{m,d-1}(i)| &= |\mathbf{A}_{m,d-1}(i, :)\boldsymbol{\phi}_{m,d-1} - \mathbf{a}_{d-1}(i)| \\ &= |[\mathbf{A}_{m,d-1}(i, :)\ \mathbf{a}_{d-1}(i)] [\boldsymbol{\phi}_{m,d-1}^\top \ -1]^\top| \\ &= |\mathbf{A}_{m,d}(i, :)\ [\boldsymbol{\phi}_{m,d-1}^\top \ -1]^\top| \\ &\leq \sqrt{\|\boldsymbol{\phi}_{m,d-1}\|^2 + 1} \|\mathbf{A}_{m,d}(i, :)\| \\ &\leq \sqrt{\|\boldsymbol{\phi}_{m,d-1}\|^2 + 1} \|\mathbf{A}_{m,d}\| \sqrt{\ell_{m,d}(i)}.\end{aligned}$$

Inequality (27b) can be obtained analogously by exchanging $\hat{\boldsymbol{\phi}}_{m,d-1}$ for $\boldsymbol{\phi}_{m,d-1}$.

Considering Inequality (27c), from Theorem 3, Lemma 3, and (27b), we have

$$\begin{aligned}|\hat{\hat{\mathbf{r}}}_{m,d-1}(i)| &= |\hat{\hat{\mathbf{A}}}_{m,d-1}(i, :)\hat{\hat{\boldsymbol{\phi}}}_{m,d-1} - \mathbf{a}_{d-1}(i)| \\ &\leq |\hat{\hat{\mathbf{A}}}_{m,d-1}(i, :)\hat{\hat{\boldsymbol{\phi}}}_{m,d-1} - \mathbf{A}_{m,d-1}(i, :)\hat{\boldsymbol{\phi}}_{m,d-1}| + |\mathbf{A}_{m,d-1}(i, :)\hat{\boldsymbol{\phi}}_{m,d-1} - \mathbf{a}_{d-1}(i)| \\ &\leq \varepsilon_2 \|\mathbf{A}_{m,d-1}(i, :)\| \|\hat{\boldsymbol{\phi}}_{m,d-1}\| + |\hat{\mathbf{r}}_{m,d-1}(i)| \\ &\leq \varepsilon_2 \|\mathbf{A}_{m,d-1}\| \sqrt{\ell_{m,d-1}(i)} \|\hat{\boldsymbol{\phi}}_{m,d-1}\| + \|\mathbf{A}_{m,d}\| \sqrt{\ell_{m,d}(i)} \sqrt{\|\hat{\boldsymbol{\phi}}_{m,d-1}\|^2 + 1} \\ &\leq \varepsilon_2 \|\mathbf{A}_{m,d}\| \sqrt{\ell_{m,d}(i)} \sqrt{\|\hat{\boldsymbol{\phi}}_{m,d-1}\|^2 + 1} + \|\mathbf{A}_{m,d}\| \sqrt{\ell_{m,d}(i)} \sqrt{\|\hat{\boldsymbol{\phi}}_{m,d-1}\|^2 + 1}\end{aligned}$$

$$= (1 + \varepsilon_2) \|\mathbf{A}_{m,d}\| \sqrt{\ell_{m,d}(i)} \sqrt{\|\hat{\phi}_{m,d-1}\|^2 + 1}.$$

□

Lemma 5. For $\mathbf{A}_{m,d} \in \mathbb{R}^{m,d}$, we have

$$|\mathbf{r}_{m,d}(i) - \hat{\mathbf{r}}_{m,d}(i)| \leq \|\mathbf{A}_{m,d}\| \sqrt{\ell_{m,d}(i)} \left(\sqrt{\varepsilon_1} \eta_{m,d} \|\phi_{m,d}\| + \varepsilon_2 \|\hat{\phi}_{m,d}\| \right),$$

for $i = 1, \dots, m$, where $\eta_{m,d}$ and ε_1 are both defined in Theorem 2, ε_2 is given in Theorem 3, and $\phi_{m,d}$, $\mathbf{r}_{m,d}$, $\hat{\phi}_{m,d}$, and $\hat{\mathbf{r}}_{m,d}$ are introduced respectively in (11), (12), (14) and (16).

Proof. Firstly, consider $|\mathbf{r}_{m,d}(i) - \hat{\mathbf{r}}_{m,d}(i)|$ and use Theorem 2 and Lemma 3 to obtain

$$\begin{aligned} |\mathbf{r}_{m,d}(i) - \hat{\mathbf{r}}_{m,d}(i)| &= \left| (\mathbf{A}_{m,d}(i, :) \phi_{m,d} - \mathbf{a}_d(i)) - (\mathbf{A}_{m,d}(i, :) \hat{\phi}_{m,d} - \mathbf{a}_d(i)) \right| \\ &= \left| \mathbf{A}_{m,d}(i, :) \phi_{m,d} - \mathbf{A}_{m,d}(i, :) \hat{\phi}_{m,d} \right| \\ &\leq \|\mathbf{A}_{m,d}(i, :)\| \|\phi_{m,d} - \hat{\phi}_{m,d}\| \\ &\leq \sqrt{\varepsilon_1} \eta_{m,d} \|\phi_{m,d}\| \|\mathbf{A}_{m,d}(i, :)\| \\ &\leq \sqrt{\varepsilon_1} \eta_{m,d} \|\phi_{m,d}\| \|\mathbf{A}_{m,d}\| \sqrt{\ell_{m,d}(i)}. \end{aligned} \quad (28)$$

Secondly, consider $|\hat{\mathbf{r}}_{m,d}(i) - \hat{\hat{\mathbf{r}}}_{m,d}(i)|$ and use Theorem 3 and Lemma 3 to obtain

$$\begin{aligned} |\hat{\mathbf{r}}_{m,d}(i) - \hat{\hat{\mathbf{r}}}_{m,d}(i)| &= \left| (\mathbf{A}_{m,d}(i, :) \hat{\phi}_{m,d} - \mathbf{a}_d(i)) - (\hat{\mathbf{A}}_{m,d}(i, :) \hat{\hat{\phi}}_{m,d} - \mathbf{a}_d(i)) \right| \\ &= \left| \mathbf{A}_{m,d}(i, :) \hat{\phi}_{m,d} - \hat{\mathbf{A}}_{m,d}(i, :) \hat{\hat{\phi}}_{m,d} \right| \\ &\leq \varepsilon_2 \|\hat{\phi}_{m,d}\| \|\mathbf{A}_{m,d}(i, :)\| \\ &\leq \varepsilon_2 \|\hat{\phi}_{m,d}\| \|\mathbf{A}_{m,d}\| \sqrt{\ell_{m,d}(i)}. \end{aligned} \quad (29)$$

Now incorporating (28) and (29), we have

$$\begin{aligned} |\mathbf{r}_{m,d}(i) - \hat{\hat{\mathbf{r}}}_{m,d}(i)| &\leq |\mathbf{r}_{m,d}(i) - \hat{\mathbf{r}}_{m,d}(i)| + |\hat{\mathbf{r}}_{m,d}(i) - \hat{\hat{\mathbf{r}}}_{m,d}(i)| \\ &\leq \sqrt{\varepsilon_1} \eta_{m,d} \|\phi_{m,d}\| \|\mathbf{A}_{m,d}\| \sqrt{\ell_{m,d}(i)} + \varepsilon_2 \|\hat{\phi}_{m,d}\| \|\mathbf{A}_{m,d}\| \sqrt{\ell_{m,d}(i)} \\ &= \|\mathbf{A}_{m,d}\| \sqrt{\ell_{m,d}(i)} \left(\sqrt{\varepsilon_1} \eta_{m,d} \|\phi_{m,d}\| + \varepsilon_2 \|\hat{\phi}_{m,d}\| \right). \end{aligned}$$

□

Lemma 6. Suppose $\mathbf{r}_{m,d}$ and $\hat{\mathbf{r}}_{m,d}$ are defined as in (12) and (15), respectively. Then, we have

$$\|\mathbf{r}_{m,d-1}\| \geq \sigma_{\min}(\mathbf{A}_{m,d})\sqrt{(\|\boldsymbol{\phi}_{m,d-1}\|^2 + 1)}, \quad (30a)$$

$$\|\hat{\mathbf{r}}_{m,d-1}\| \geq \sigma_{\min}(\mathbf{A}_{m,d})\sqrt{(\|\hat{\boldsymbol{\phi}}_{m,d-1}\|^2 + 1)}, \quad (30b)$$

where $\sigma_{\min}(\cdot)$ denotes the minimum singular value, and $\boldsymbol{\phi}_{m,d}$, $\mathbf{r}_{m,d}$, $\hat{\boldsymbol{\phi}}_{m,d}$, and $\hat{\mathbf{r}}_{m,d}$ are given respectively in (11), (12), (14) and (15).

Proof. By definition of the residual, we have

$$\begin{aligned} \|\mathbf{r}_{m,d-1}\| &= \|\mathbf{A}_{m,d-1}\boldsymbol{\phi}_{m,d-1} - \mathbf{a}_{d-1}\| \\ &= \left\| \begin{bmatrix} \mathbf{A}_{m,d-1} & \mathbf{a}_{d-1} \end{bmatrix} \begin{bmatrix} \boldsymbol{\phi}_{m,d-1}^\top & -1 \end{bmatrix}^\top \right\| \\ &= \left\| \mathbf{A}_{m,d} \begin{bmatrix} \boldsymbol{\phi}_{m,d-1}^\top & -1 \end{bmatrix}^\top \right\| \\ &= \sqrt{\begin{bmatrix} \boldsymbol{\phi}_{m,d-1}^\top & -1 \end{bmatrix} \mathbf{A}_{m,d}^\top \mathbf{A}_{m,d} \begin{bmatrix} \boldsymbol{\phi}_{m,d-1}^\top & -1 \end{bmatrix}^\top} \\ &= \sqrt{\frac{\begin{bmatrix} \boldsymbol{\phi}_{m,d-1}^\top & -1 \end{bmatrix} \mathbf{A}_{m,d}^\top \mathbf{A}_{m,d} \begin{bmatrix} \boldsymbol{\phi}_{m,d-1}^\top & -1 \end{bmatrix}^\top}{\left\| \begin{bmatrix} \boldsymbol{\phi}_{m,d-1}^\top & -1 \end{bmatrix} \right\|^2}} \left\| \begin{bmatrix} \boldsymbol{\phi}_{m,d-1}^\top & -1 \end{bmatrix} \right\|^2} \\ &\geq \sigma_{\min}(\mathbf{A}_{m,d})\sqrt{\|\boldsymbol{\phi}_{m,d-1}\|^2 + 1}. \end{aligned}$$

Inequality (30b) is shown analogously. \square

Lemma 7. Suppose $\hat{\mathbf{r}}_{m,d}$ and $\hat{\hat{\mathbf{r}}}_{m,d}$ are defined as in (15) and (16), respectively. Then, we have

$$\|\hat{\mathbf{r}}_{m,d} - \hat{\hat{\mathbf{r}}}_{m,d}\| \leq \varepsilon_2 \kappa(\mathbf{A}_{m,d})\sqrt{d}\|\hat{\mathbf{r}}_{m,d}\|,$$

where $\kappa(\cdot)$ denotes the condition number, and ε_2 is as given in Theorem 3.

Proof. Using Lemma 6, (15) and (16), and Theorem 3 we obtain

$$\begin{aligned} \|\hat{\mathbf{r}}_{m,d} - \hat{\hat{\mathbf{r}}}_{m,d}\| &= \|\hat{\mathbf{r}}_{m,d} - \hat{\hat{\mathbf{r}}}_{m,d}\|_F \\ &= \|(\mathbf{A}_{m,d}\hat{\boldsymbol{\phi}}_{m,d} - \mathbf{a}_d) - (\hat{\mathbf{A}}_{m,d}\hat{\hat{\boldsymbol{\phi}}}_{m,d} - \mathbf{a}_d)\|_F \\ &= \|\mathbf{A}_{m,d}\hat{\boldsymbol{\phi}}_{m,d} - \hat{\mathbf{A}}_{m,d}\hat{\hat{\boldsymbol{\phi}}}_{m,d}\|_F \\ &\leq \varepsilon_2 \|\mathbf{A}_{m,d}\|_F \left\| \hat{\boldsymbol{\phi}}_{m,d} \right\| \\ &\leq \varepsilon_2 \|\mathbf{A}_{m,d}\|_F \sqrt{\|\hat{\boldsymbol{\phi}}_{m,d}\|^2 + 1} \end{aligned}$$

$$\begin{aligned}
&\leq \varepsilon_2 \sqrt{d} \|\mathbf{A}_{m,d}\| \frac{\|\hat{\mathbf{r}}_{m,d}\|}{\sigma_{\min}(\mathbf{A}_{m,d})} \\
&\leq \varepsilon_2 \kappa(\mathbf{A}_{m,d}) \sqrt{d} \|\hat{\mathbf{r}}_{m,d}\|.
\end{aligned}$$

□

Lemma 8. Suppose $\mathbf{r}_{m,d}$ and $\hat{\mathbf{r}}_{m,d}$ are defined as in (12) and (16), respectively. Then, we have

$$\|\hat{\mathbf{r}}_{m,d}\| \leq (1 + \varepsilon^* \xi_{m,d}) \|\mathbf{r}_{m,d}\|,$$

where $\varepsilon^* = \max\{\varepsilon_1, \varepsilon_2\}$, and ε_1 and ε_2 are as in Theorems 2 and 3 and $\xi_{m,d}$ is as in Theorem 4.

Proof. From Lemma 7, we obtain

$$\begin{aligned}
\left| \|\hat{\mathbf{r}}_{m,d}\| - \|\hat{\hat{\mathbf{r}}}_{m,d}\| \right| &\leq \|\hat{\mathbf{r}}_{m,d} - \hat{\hat{\mathbf{r}}}_{m,d}\| \\
&\leq \varepsilon_2 \kappa(\mathbf{A}_{m,d}) \sqrt{d} \|\hat{\mathbf{r}}_{m,d}\|.
\end{aligned} \tag{31}$$

By rearranging (31) and using Theorem 2, we have

$$\begin{aligned}
\|\hat{\hat{\mathbf{r}}}_{m,d}\| &\leq (1 + \varepsilon_2 \kappa(\mathbf{A}_{m,d}) \sqrt{d}) \|\hat{\mathbf{r}}_{m,d}\| \\
&\leq (1 + \varepsilon_2 \kappa(\mathbf{A}_{m,d}) \sqrt{d}) (1 + \varepsilon_1) \|\mathbf{r}_{m,d}\| \\
&= \left(1 + \varepsilon_1 + \varepsilon_2 \kappa(\mathbf{A}_{m,d}) \sqrt{d} \right) + \varepsilon_1 \varepsilon_2 \kappa(\mathbf{A}_{m,d}) \sqrt{d} \|\mathbf{r}_{m,d}\| \\
&\leq \left(1 + \varepsilon^* + \varepsilon^* \kappa(\mathbf{A}_{m,d}) \sqrt{d} \right) + \varepsilon^* \kappa(\mathbf{A}_{m,d}) \sqrt{d} \|\mathbf{r}_{m,d}\| \\
&= \left(1 + \varepsilon^* (1 + 2\kappa(\mathbf{A}_{m,d}) \sqrt{d}) \right) \|\mathbf{r}_{m,d}\| \\
&= (1 + \varepsilon^* \xi_{m,d}) \|\mathbf{r}_{m,d}\|.
\end{aligned}$$

□

Proof of Theorem 4

Proof. We prove this theorem by induction for the two cases $1 \leq d \leq s_2$ and $s_2 \leq d < n$.

Case 1: $1 \leq d \leq s_2$. The statement is trivial for $d = 1$, as $\hat{\ell}_{m,1} = \ell_{m,1}$. Now let us assume the statement of Theorem 4 is true for all $d < \bar{d}$ for some $\bar{d} \leq s_2$, and prove it is also true for $d = \bar{d}$.

Using the induction hypothesis along with Theorem 1 and Definition 1, we have

$$\left| \ell_{m,\bar{d}}(i) - \hat{\ell}_{m,\bar{d}}(i) \right| = \left| \ell_{m,\bar{d}-1}(i) + \frac{(\mathbf{r}_{m,\bar{d}-1}(i))^2}{\|\mathbf{r}_{m,\bar{d}-1}\|^2} - \hat{\ell}_{m,\bar{d}-1}(i) - \frac{(\hat{\mathbf{r}}_{m,\bar{d}-1}(i))^2}{\|\hat{\mathbf{r}}_{m,\bar{d}-1}\|^2} \right|$$

$$\begin{aligned}
& \leq \left| \ell_{m,\bar{d}-1}(i) - \hat{\ell}_{m,\bar{d}-1}(i) \right| \\
& \quad + \left| \frac{(\mathbf{r}_{m,\bar{d}-1}(i))^2}{\|\mathbf{r}_{m,\bar{d}-1}\|^2} - \frac{(\mathbf{r}_{m,\bar{d}-1}(i))^2}{\|\hat{\mathbf{r}}_{m,\bar{d}-1}\|^2} + \frac{(\mathbf{r}_{m,\bar{d}-1}(i))^2}{\|\hat{\mathbf{r}}_{m,\bar{d}-1}\|^2} - \frac{(\hat{\mathbf{r}}_{m,\bar{d}-1}(i))^2}{\|\hat{\mathbf{r}}_{m,\bar{d}-1}\|^2} \right| \\
& \leq \left(\sqrt{\xi_{m,\bar{d}-2}} + 5(\eta_{m,\bar{d}-2} + 2)\kappa^2(\mathbf{A}_{m,\bar{d}-1}) \right) (\bar{d} - 2) \sqrt{\varepsilon^*} \ell_{m,\bar{d}-1}(i) \\
& \quad + (\mathbf{r}_{m,\bar{d}-1}(i))^2 \left| \frac{1}{\|\mathbf{r}_{m,\bar{d}-1}\|^2} - \frac{1}{\|\hat{\mathbf{r}}_{m,\bar{d}-1}\|^2} \right| + \frac{1}{\|\hat{\mathbf{r}}_{m,\bar{d}-1}\|^2} \left| (\mathbf{r}_{m,\bar{d}-1}(i))^2 - (\hat{\mathbf{r}}_{m,\bar{d}-1}(i))^2 \right|.
\end{aligned}$$

Now, by using Theorem 2, we have

$$\begin{aligned}
\left| \ell_{m,\bar{d}}(i) - \hat{\ell}_{m,\bar{d}}(i) \right| & \leq \left(\sqrt{\xi_{m,\bar{d}-2}} + 5(\eta_{m,\bar{d}-2} + 2)\kappa^2(\mathbf{A}_{m,\bar{d}-1}) \right) (\bar{d} - 2) \sqrt{\varepsilon^*} \ell_{m,\bar{d}-1}(i) \\
& \quad + (\mathbf{r}_{m,\bar{d}-1}(i))^2 \left| \frac{1}{\|\mathbf{r}_{m,\bar{d}-1}\|^2} - \frac{1}{(1 + \varepsilon_1)^2 \|\mathbf{r}_{m,\bar{d}-1}\|^2} \right| \\
& \quad + \frac{1}{\|\mathbf{r}_{m,\bar{d}-1}\|^2} \left| (\mathbf{r}_{m,\bar{d}-1}(i) - \hat{\mathbf{r}}_{m,\bar{d}-1}(i)) \right| \left| (\mathbf{r}_{m,\bar{d}-1}(i) + \hat{\mathbf{r}}_{m,\bar{d}-1}(i)) \right| \\
& \leq \left(\sqrt{\xi_{m,\bar{d}-2}} + 5(\eta_{m,\bar{d}-2} + 2)\kappa^2(\mathbf{A}_{m,\bar{d}-1}) \right) (\bar{d} - 2) \sqrt{\varepsilon^*} \ell_{m,\bar{d}-1}(i) + \frac{\varepsilon_1^2 + 2\varepsilon_1}{(1 + \varepsilon_1)^2} \frac{(\mathbf{r}_{m,\bar{d}-1}(i))^2}{\|\mathbf{r}_{m,\bar{d}-1}\|^2} \\
& \quad + \frac{1}{\|\mathbf{r}_{m,\bar{d}-1}\|^2} \left| (\mathbf{r}_{m,\bar{d}-1}(i) - \hat{\mathbf{r}}_{m,\bar{d}-1}(i)) \right| \left(\left| \mathbf{r}_{m,\bar{d}-1}(i) \right| + \left| \hat{\mathbf{r}}_{m,\bar{d}-1}(i) \right| \right).
\end{aligned}$$

From Theorem 1, we have

$$\ell_{m,\bar{d}-1}(i) \leq \ell_{m,\bar{d}}(i) \text{ and} \quad (32a)$$

$$\frac{(\mathbf{r}_{m,\bar{d}-1}(i))^2}{\|\mathbf{r}_{m,\bar{d}-1}\|^2} \leq \ell_{m,\bar{d}}(i) \quad (32b)$$

for $i = 1, \dots, m$ and $2 \leq \bar{d} \leq s_2$. Considering (32a) and (32b) as well as using (28) and Lemma 4, we now have

$$\begin{aligned}
\left| \ell_{m,\bar{d}}(i) - \hat{\ell}_{m,\bar{d}}(i) \right| & \leq \left(\sqrt{\xi_{m,\bar{d}-2}} + 5(\eta_{m,\bar{d}-2} + 2)\kappa^2(\mathbf{A}_{m,\bar{d}-1}) \right) (\bar{d} - 2) \sqrt{\varepsilon^*} \ell_{m,\bar{d}}(i) + \frac{\varepsilon_1^2 + 2\varepsilon_1}{(1 + \varepsilon_1)^2} \ell_{m,\bar{d}}(i) \\
& \quad + \frac{1}{\|\mathbf{r}_{m,\bar{d}-1}\|^2} \left(\sqrt{\varepsilon_1} \eta_{m,\bar{d}-1} \|\phi_{m,\bar{d}-1}\| \|\mathbf{A}_{m,\bar{d}-1}\| \sqrt{\ell_{m,\bar{d}-1}(i)} \right) \\
& \quad \times \left(\sqrt{\|\phi_{m,\bar{d}-1}\|^2 + 1} \|\mathbf{A}_{m,\bar{d}}\| \sqrt{\ell_{m,\bar{d}}(i)} + \sqrt{\|\hat{\phi}_{m,\bar{d}-1}\|^2 + 1} \|\mathbf{A}_{m,\bar{d}}\| \sqrt{\ell_{m,\bar{d}}(i)} \right) \\
& \leq \left(\sqrt{\xi_{m,\bar{d}-2}} + 5(\eta_{m,\bar{d}-2} + 2)\kappa^2(\mathbf{A}_{m,\bar{d}-1}) \right) (\bar{d} - 2) \sqrt{\varepsilon^*} \ell_{m,\bar{d}-1}(i) + \left(\frac{\sqrt{\varepsilon_1}(2 + \varepsilon_1)}{(1 + \varepsilon_1)^2} \right) \\
& \quad + \frac{\eta_{m,\bar{d}-1} \|\phi_{m,\bar{d}-1}\| \|\mathbf{A}_{m,\bar{d}-1}\| \|\mathbf{A}_{m,\bar{d}}\|}{\|\mathbf{r}_{m,\bar{d}-1}\|^2} \left(\sqrt{\|\phi_{m,\bar{d}-1}\|^2 + 1} + \sqrt{\|\hat{\phi}_{m,\bar{d}-1}\|^2 + 1} \right) \sqrt{\varepsilon_1} \ell_{m,\bar{d}}(i).
\end{aligned}$$

One can easily see that for a given $0 < \varepsilon_1 < 1$, we have

$$\frac{\sqrt{\varepsilon_1}(2 + \varepsilon_1)}{(1 + \varepsilon_1)^2} \leq \frac{\sqrt{\varepsilon_1}(2 + 2\varepsilon_1)}{(1 + \varepsilon_1)^2} = \frac{2\sqrt{\varepsilon_1}}{1 + \varepsilon_1} \leq 1. \quad (33)$$

Additionally, $\|\mathbf{A}_{m,\bar{d}-1}\| \leq \|\mathbf{A}_{m,\bar{d}}\|$ and $\kappa(\mathbf{A}_{m,\bar{d}-1}) \leq \kappa(\mathbf{A}_{m,\bar{d}})$ (equivalently, $\eta_{m,\bar{d}-1} \leq \eta_{m,\bar{d}}$) for all $2 \leq \bar{d} \leq s_2$, and using Theorem 2 and Lemma 6, we can obtain

$$\begin{aligned}
\left| \ell_{m,\bar{d}}(i) - \hat{\ell}_{m,\bar{d}}(i) \right| &\leq \left(\sqrt{\xi_{m,\bar{d}-2}} + 5(\eta_{m,\bar{d}-1} + 2)\kappa^2(\mathbf{A}_{m,\bar{d}}) \right) (\bar{d} - 2) \sqrt{\varepsilon^*} \ell_{m,\bar{d}}(i) \\
&\quad + \left(1 + \frac{\eta_{m,\bar{d}-1} \sqrt{\|\boldsymbol{\phi}_{m,\bar{d}-1}\|^2 + 1} \|\mathbf{A}_{m,\bar{d}}\|^2}{\|\mathbf{r}_{m,\bar{d}-1}\|} \right. \\
&\quad \quad \left. \times \left(\frac{\sqrt{\|\boldsymbol{\phi}_{m,\bar{d}-1}\|^2 + 1}}{\|\mathbf{r}_{m,\bar{d}-1}\|} + \frac{\sqrt{\|\hat{\boldsymbol{\phi}}_{m,\bar{d}-1}\|^2 + 1}}{\|\mathbf{r}_{m,\bar{d}-1}\|} \right) \right) \sqrt{\varepsilon^*} \ell_{m,\bar{d}}(i) \\
&\leq \left(\sqrt{\xi_{m,\bar{d}-2}} + 5(\eta_{m,\bar{d}-1} + 2)\kappa^2(\mathbf{A}_{m,\bar{d}}) \right) (\bar{d} - 2) \sqrt{\varepsilon^*} \ell_{m,\bar{d}}(i) \\
&\quad + \left(1 + \frac{\eta_{m,\bar{d}-1} \sqrt{\|\boldsymbol{\phi}_{m,\bar{d}-1}\|^2 + 1} \|\mathbf{A}_{m,\bar{d}}\|^2}{\|\mathbf{r}_{m,\bar{d}-1}\|} \right. \\
&\quad \quad \left. \times \left(\frac{\sqrt{\|\boldsymbol{\phi}_{m,\bar{d}-1}\|^2 + 1}}{\|\mathbf{r}_{m,\bar{d}-1}\|} + \frac{(1 + \varepsilon_1) \sqrt{\|\hat{\boldsymbol{\phi}}_{m,\bar{d}-1}\|^2 + 1}}{\|\hat{\mathbf{r}}_{m,\bar{d}-1}\|} \right) \right) \sqrt{\varepsilon^*} \ell_{m,\bar{d}}(i) \\
&\leq \left(\sqrt{\xi_{m,\bar{d}-2}} + 5(\eta_{m,\bar{d}-1} + 2)\kappa^2(\mathbf{A}_{m,\bar{d}}) \right) (\bar{d} - 2) \sqrt{\varepsilon^*} \ell_{m,\bar{d}}(i) \\
&\quad + \left(1 + \frac{\eta_{m,\bar{d}-1} \|\mathbf{A}_{m,\bar{d}}\|^2}{\sigma_{\min}(\mathbf{A}_{m,\bar{d}})} \left(\frac{1}{\sigma_{\min}(\mathbf{A}_{m,\bar{d}})} + \frac{1 + \varepsilon_1}{\sigma_{\min}(\mathbf{A}_{m,\bar{d}})} \right) \right) \sqrt{\varepsilon^*} \ell_{m,\bar{d}}(i) \\
&\leq \left(\sqrt{\xi_{m,\bar{d}-2}} + 5(\eta_{m,\bar{d}-1} + 2)\kappa^2(\mathbf{A}_{m,\bar{d}}) \right) (\bar{d} - 2) \sqrt{\varepsilon^*} \ell_{m,\bar{d}}(i) \\
&\quad + (1 + 3\eta_{m,\bar{d}-1} \kappa^2(\mathbf{A}_{m,\bar{d}})) \sqrt{\varepsilon^*} \ell_{m,\bar{d}}(i).
\end{aligned}$$

One can easily see $1 < \xi_{m,\bar{d}-2} \leq \xi_{m,\bar{d}-1}$, implying

$$\left| \ell_{m,\bar{d}}(i) - \hat{\ell}_{m,\bar{d}}(i) \right| \leq \left(\sqrt{\xi_{m,\bar{d}-1}} + 5(\eta_{m,\bar{d}-1} + 2)\kappa^2(\mathbf{A}_{m,\bar{d}}) \right) (\bar{d} - 1) \sqrt{\varepsilon^*} \ell_{m,\bar{d}}(i).$$

Thus, Theorem 4 holds for $1 \leq d \leq s_2$ by induction.

Case 2: $s_2 \leq d < n$. Now we suppose Theorem 4 holds for all $d < \bar{d}$ for some $s_2 \leq \bar{d} < n$, and prove it is also true for $d = \bar{d}$.

Analogous to Case 1 and using the induction hypothesis along with Theorem 1 and Definition 1, we have

$$\begin{aligned}
\left| \ell_{m,\bar{d}}(i) - \hat{\ell}_{m,\bar{d}}(i) \right| &\leq \left(\sqrt{\xi_{m,\bar{d}-2}} + 5(\eta_{m,\bar{d}-2} + 2)\kappa^2(\mathbf{A}_{m,\bar{d}-1}) \right) (\bar{d} - 2) \sqrt{\varepsilon^*} \ell_{m,\bar{d}-1}(i) \\
&\quad + (\mathbf{r}_{m,\bar{d}-1}(i))^2 \left| \frac{1}{\|\mathbf{r}_{m,\bar{d}-1}\|^2} - \frac{1}{\|\hat{\mathbf{r}}_{m,\bar{d}-1}\|^2} \right| \\
&\quad + \frac{1}{\|\hat{\mathbf{r}}_{m,\bar{d}-1}\|^2} \left| (\mathbf{r}_{m,\bar{d}-1}(i))^2 - (\hat{\mathbf{r}}_{m,\bar{d}-1}(i))^2 \right|.
\end{aligned}$$

Using Lemmas 4 to 6 and 8, we obtain

$$\begin{aligned}
|\ell_{m,\bar{d}}(i) - \hat{\ell}_{m,\bar{d}}(i)| &\leq \left(\sqrt{\xi_{m,\bar{d}-2}} + 5(\eta_{m,\bar{d}-2} + 2)\kappa^2(\mathbf{A}_{m,\bar{d}-1}) \right) (\bar{d} - 2) \sqrt{\varepsilon^*} \ell_{m,\bar{d}-1}(i) \\
&\quad + (\mathbf{r}_{m,\bar{d}-1}(i))^2 \left| \frac{1}{\|\mathbf{r}_{m,\bar{d}-1}\|^2} - \frac{1}{(1 + \varepsilon^* \xi_{m,\bar{d}-1})^2 \|\mathbf{r}_{m,\bar{d}-1}\|^2} \right| \\
&\quad + \frac{1}{\|\mathbf{r}_{m,\bar{d}-1}\|^2} \left| \mathbf{r}_{m,\bar{d}-1}(i) - \hat{\mathbf{r}}_{m,\bar{d}-1}(i) \right| \left| \mathbf{r}_{m,\bar{d}-1}(i) + \hat{\mathbf{r}}_{m,\bar{d}-1}(i) \right| \\
&\leq \left(\sqrt{\xi_{m,\bar{d}-2}} + 5(\eta_{m,\bar{d}-2} + 2)\kappa^2(\mathbf{A}_{m,\bar{d}-1}) \right) (\bar{d} - 2) \sqrt{\varepsilon^*} \ell_{m,\bar{d}-1}(i) \\
&\quad + \left(\frac{(\varepsilon^* \xi_{m,\bar{d}-1})^2 + 2\varepsilon^* \xi_{m,\bar{d}-1}}{(1 + \varepsilon^* \xi_{m,\bar{d}-1})^2} \right) \frac{(\mathbf{r}_{m,\bar{d}-1}(i))^2}{\|\mathbf{r}_{m,\bar{d}-1}\|^2} \\
&\quad + \frac{1}{\|\mathbf{r}_{m,\bar{d}-1}\|^2} \|\mathbf{A}_{m,\bar{d}-1}\| \sqrt{\ell_{m,\bar{d}-1}(i)} \left(\sqrt{\varepsilon_1} \eta_{m,\bar{d}-1} \|\phi_{m,\bar{d}-1}\| + \varepsilon_2 \|\hat{\phi}_{m,\bar{d}-1}\| \right) \\
&\quad \times \left(\sqrt{\|\phi_{m,\bar{d}-1}\|^2 + 1} \|\mathbf{A}_{m,\bar{d}}\| \sqrt{\ell_{m,\bar{d}}(i)} + (1 + \varepsilon_2) \sqrt{\|\hat{\phi}_{m,\bar{d}-1}\|^2 + 1} \|\mathbf{A}_{m,\bar{d}}\| \sqrt{\ell_{m,\bar{d}}(i)} \right) \\
&\leq \left(\sqrt{\xi_{m,\bar{d}-2}} + 5(\eta_{m,\bar{d}-2} + 2)\kappa^2(\mathbf{A}_{m,\bar{d}-1}) \right) (\bar{d} - 2) \sqrt{\varepsilon^*} \ell_{m,\bar{d}-1}(i) \\
&\quad + \left(\frac{(\varepsilon^* \xi_{m,\bar{d}-1})^2 + 2\varepsilon^* \xi_{m,\bar{d}-1}}{(1 + \varepsilon^* \xi_{m,\bar{d}-1})^2} \right) \ell_{m,\bar{d}-1}(i) \\
&\quad + \|\mathbf{A}_{m,\bar{d}-1}\| \sqrt{\ell_{m,\bar{d}-1}(i)} \left(\sqrt{\varepsilon_1} \eta_{m,\bar{d}-1} \frac{\sqrt{\|\phi_{m,\bar{d}-1}\|^2 + 1}}{\|\mathbf{r}_{m,\bar{d}-1}\|} + \varepsilon_2 \frac{\sqrt{\|\hat{\phi}_{m,\bar{d}-1}\|^2 + 1}}{\|\mathbf{r}_{m,\bar{d}-1}\|} \right) \\
&\quad \times \left(\frac{\sqrt{\|\phi_{m,\bar{d}-1}\|^2 + 1}}{\|\mathbf{r}_{m,\bar{d}-1}\|} \|\mathbf{A}_{m,\bar{d}}\| \sqrt{\ell_{m,\bar{d}}(i)} + (1 + \varepsilon_2) \frac{\sqrt{\|\hat{\phi}_{m,\bar{d}-1}\|^2 + 1}}{\|\mathbf{r}_{m,\bar{d}-1}\|} \|\mathbf{A}_{m,\bar{d}}\| \sqrt{\ell_{m,\bar{d}}(i)} \right) \\
&\leq \left(\sqrt{\xi_{m,\bar{d}-2}} + 5(\eta_{m,\bar{d}-1} + 2)\kappa^2(\mathbf{A}_{m,\bar{d}}) \right) (\bar{d} - 2) \sqrt{\varepsilon^*} \ell_{m,\bar{d}}(i) \\
&\quad + \left(\frac{(\varepsilon^* \xi_{m,\bar{d}-1})^2 + 2\varepsilon^* \xi_{m,\bar{d}-1}}{(1 + \varepsilon^* \xi_{m,\bar{d}-1})^2} \right) \ell_{m,\bar{d}-1}(i) \\
&\quad + \|\mathbf{A}_{m,\bar{d}}\|^2 \left(\sqrt{\varepsilon_1} \eta_{m,\bar{d}-1} \frac{1}{\sigma_{\min}(\mathbf{A}_{m,\bar{d}})} + \varepsilon_2 (1 + \varepsilon_1) \frac{1}{\sigma_{\min}(\mathbf{A}_{m,\bar{d}})} \right) \\
&\quad \quad \times \left(\frac{1}{\sigma_{\min}(\mathbf{A}_{m,\bar{d}})} + (1 + \varepsilon_2)(1 + \varepsilon_1) \frac{1}{\sigma_{\min}(\mathbf{A}_{m,\bar{d}})} \right) \ell_{m,\bar{d}}(i) \\
&\leq \left(\sqrt{\xi_{m,\bar{d}-2}} + 5(\eta_{m,\bar{d}-1} + 2)\kappa^2(\mathbf{A}_{m,\bar{d}}) \right) (\bar{d} - 2) \sqrt{\varepsilon^*} \ell_{m,\bar{d}}(i) \\
&\quad + \left(\frac{2\sqrt{\varepsilon^* \xi_{m,\bar{d}-1}}}{1 + \varepsilon^* \xi_{m,\bar{d}-1}} \right) \sqrt{\xi_{m,\bar{d}-1}} \sqrt{\varepsilon^*} \ell_{m,\bar{d}}(i) \\
&\quad + \|\mathbf{A}_{m,\bar{d}}\|^2 \left(\sqrt{\varepsilon^*} \eta_{m,\bar{d}-1} \frac{1}{\sigma_{\min}(\mathbf{A}_{m,\bar{d}})} + \varepsilon^* (1 + \varepsilon^*) \frac{1}{\sigma_{\min}(\mathbf{A}_{m,\bar{d}})} \right)
\end{aligned}$$

$$\begin{aligned}
& \times \left(\frac{1}{\sigma_{\min}(\mathbf{A}_{m,\bar{d}})} + (1 + \varepsilon^*)(1 + \varepsilon^*) \frac{1}{\sigma_{\min}(\mathbf{A}_{m,\bar{d}})} \right) \ell_{m,\bar{d}}(i) \\
& \leq \left(\sqrt{\xi_{m,\bar{d}-2}} + 5(\eta_{m,\bar{d}-1} + 2)\kappa^2(\mathbf{A}_{m,\bar{d}}) \right) (\bar{d} - 2) \sqrt{\varepsilon^*} \ell_{m,\bar{d}}(i) \\
& \quad + \left(\sqrt{\xi_{m,\bar{d}-1}} + 5(\eta_{m,\bar{d}-1} + 2)\kappa(\mathbf{A}_{m,\bar{d}})^2 \right) \sqrt{\varepsilon^*} \ell_{m,\bar{d}}(i).
\end{aligned}$$

$\xi_{m,d}$ is an increasing function in d , we have

$$|\ell_{m,\bar{d}}(i) - \hat{\ell}_{m,\bar{d}}(i)| \leq \left(\sqrt{\xi_{m,\bar{d}-1}} + 5(\eta_{m,\bar{d}-1} + 2)\kappa^2(\mathbf{A}_{m,\bar{d}}) \right) (\bar{d} - 1) \sqrt{\varepsilon^*} \ell_{m,\bar{d}}(i).$$

□

References

- [1] M. Abolghasemi, J. Hurley, A. Eshragh, and B. Fahimnia. Demand forecasting in the presence of systematic events: Cases in capturing sales promotions. *International Journal of Production Economics*, 230:107892, 2020.
- [2] A. Alaoui and M. W. Mahoney. Fast randomized kernel ridge regression with statistical guarantees. *Advances in neural information processing systems*, 28, 2015.
- [3] H. Avron, P. Maymounkov, and S. Toledo. Blendenpik: Supercharging LAPACK’s least-squares solver. *SIAM Journal on Scientific Computing*, 32(3):1217–1236, 2010.
- [4] P. Broersen. Autoregressive model orders for Durbin’s MA and ARMA estimators. *Signal Processing, IEEE Transactions on*, 48:2454–2457, 2000.
- [5] L. Cella. Efficient context-aware sequential recommender system. In *Companion Proceedings of the The Web Conference 2018*, pages 1391–1394, 2018.
- [6] Y. Chen, S. Bhojanapalli, S. Sanghavi, and R. Ward. Completing any low-rank matrix, provably. *The Journal of Machine Learning Research*, 16(1):2999–3034, 2015.
- [7] Y. Chen and Y. Yang. Fast statistical leverage score approximation in kernel ridge regression. In *International Conference on Artificial Intelligence and Statistics*, pages 2935–2943. PMLR, 2021.
- [8] K. Clarkson and D. Woodruff. Low-rank approximation and regression in input sparsity time. *Journal of the ACM (JACM)*, 63(6):1–45, 2017.
- [9] M. Cohen, Y. Lee, C. Musco, C. Musco, R. Peng, and A. Sidford. Uniform sampling for matrix approximation. In *Proceedings of the 2015 Conference on Innovations in Theoretical Computer Science*, pages 181–190, 2015.

- [10] M. Cohen, C. Musco, and C. Musco. Input sparsity time low-rank approximation via ridge leverage score sampling. In *Proceedings of the Twenty-Eighth Annual ACM-SIAM Symposium on Discrete Algorithms*, pages 1758–1777. SIAM, 2017.
- [11] M. Derezhinski and M. W. Mahoney. Determinantal point processes in randomized numerical linear algebra. *Notices of the AMS*, 68(1):34–45, 2021.
- [12] P. Drineas, R. Kannan, and M. W. Mahoney. Fast Monte Carlo Algorithms for Matrices I: Approximating Matrix Multiplication. *SIAM Journal on Computing*, 36(1):132–157, 2006.
- [13] P. Drineas, M. Magdon-Ismail, M. W. Mahoney, and D.P. Woodruff. Fast approximation of matrix coherence and statistical leverage. *Journal of Machine Learning Research*, 13(Dec):3475–3506, 2012.
- [14] P. Drineas and M. W. Mahoney. RandNLA: Randomized numerical linear algebra. *Communications of the ACM*, 59:80–90, 2016.
- [15] P. Drineas and M. W. Mahoney. Lectures on randomized numerical linear algebra. In M. W. Mahoney, J. C. Duchi, and A. C. Gilbert, editors, *The Mathematics of Data*, IAS/Park City Mathematics Series, pages 1–48. AMS/IAS/SIAM, 2018.
- [16] P. Drineas, M. W. Mahoney, and S. Muthukrishnan. Sampling algorithms for ℓ_2 regression and applications. In *Proceedings of the 17th Annual ACM-SIAM Symposium on Discrete Algorithms*, pages 1127–1136, 2006.
- [17] P. Drineas, M. W. Mahoney, and S. Muthukrishnan. Relative-error CUR matrix decompositions. *SIAM Journal on Matrix Analysis and Applications*, 30:844–881, 2008.
- [18] P. Drineas, M. W. Mahoney, S. Muthukrishnan, and T. Sarlos. Faster least squares approximation. *Numerische Mathematik*, 117(2):219–249, 2011.
- [19] J. Durbin. Efficient Estimation Of Parameters In Moving-Average Models. *Biometrika*, 46(3-4):306–316, 1959.
- [20] A. Eshragh, S. Alizamir, P. Howley, and E. Stojanovski. Modeling the dynamics of the COVID-19 population in Australia: A probabilistic analysis. *PLoS ONE*, 15(10):e0240153, 2020.
- [21] A. Eshragh, B. Ganim, T. Perkins, and K. Bandara. The importance of environmental factors in forecasting Australian power demand. *Environmental Modeling & Assessment*, 27:1–11, 2022.
- [22] A. Eshragh, G. Livingston Jr, T. McCann, and L. Yerbury. Rollage: Efficient rolling average algorithm to estimate ARMA models for big time series data. *arXiv:2103.09175*, 2023.

- [23] A. Eshragh, Pietro, O.D., and M. Saunders. Toeplitz least squares problems, fast algorithms and big data. *arXiv:2112.12994*, 2021.
- [24] A. Eshragh, F. Roosta, A. Nazari, and M. W. Mahoney. LSAR: Efficient leverage score sampling algorithm for the analysis of big time series data. *Journal of Machine Learning Research*, 23:1–36, 2022.
- [25] R. Estrin, D. Orban, and M. Saunders. LSLQ: An iterative method for linear least-squares with an error minimization property. *SIAM Journal on Matrix Analysis and Applications*, 40(1):254–275, 2019.
- [26] B. Fahimnia, J. Sarkis, and A. Eshragh. A tradeoff model for green supply chain planning: A leanness-versus-greenness analysis. *Omega*, 54:173–190, 2015.
- [27] D. Fong and M. Saunders. LSMR: An iterative algorithm for sparse least-squares problems. *SIAM Journal on Scientific Computing*, 33(5):2950–2971, 2011.
- [28] G. Golub and C. Loan. *Matrix Computations*. Johns Hopkins University Press, 1983.
- [29] J. Hamilton. *Time Series Analysis*. Princeton University Press, Princeton, New Jersey, 1994.
- [30] E. Hannan and J. Rissanen. Recursive Estimation of Mixed Autoregressive-Moving Average Order. *Biometrika*, 69(1):81–94, 1982.
- [31] G. Kutyniok, M. Saunders, S. Wright, and O. Yilmaz. Sparse representations, numerical linear algebra, and optimization. 2014.
- [32] G. Li, M. and Miller and R. Peng. Iterative row sampling. In *2013 IEEE 54th Annual Symposium on Foundations of Computer Science*, pages 127–136. IEEE, 2013.
- [33] E. Liberty, F. Woolfe, P. Martinsson, V. Rokhlin, and M. Tygert. Randomized algorithms for the low-rank approximation of matrices. *Proceedings of the National Academy of Sciences*, 104(51):20167–20172, 2007.
- [34] Y. Liu and S. Zhang. Fast quantum algorithms for least squares regression and statistic leverage scores. *Theoretical Computer Science*, 657:38–47, 2017.
- [35] M. W. Mahoney. Randomized algorithms for matrices and data. *Foundations and Trends® in Machine Learning*, 2011.
- [36] M. W. Mahoney and P. Drineas. CUR matrix decompositions for improved data analysis. *Proc. Natl. Acad. Sci. USA*, 106:697–702, 2009.
- [37] X. Meng and M. W. Mahoney. Low-distortion subspace embeddings in input-sparsity time and applications to robust linear regression. In *Proceedings of the 45th Annual ACM Symposium on Theory of Computing*, pages 91–100, 2013.

- [38] X. Meng, M.A. Saunders, and M. W. Mahoney. LSRN: A parallel iterative solver for strongly over-or underdetermined systems. *SIAM Journal on Scientific Computing*, 36(2):C95–C118, 2014.
- [39] R. Murray, J. Demmel, M. W. Mahoney, N. B. Erichson, M. Melnichenko, O. A. Malik, L. Grigori, P. Luszczek, M. Dereziński, M. E. Lopes, T. Liang, H. Luo, and J. Dongarra. Randomized Numerical Linear Algebra – a perspective on the field with an eye to software. Technical Report Preprint: arXiv:2302.11474v2, 2023.
- [40] C. Musco and C. Musco. Recursive sampling for the Nystrom method. *Advances in neural information processing systems*, 30, 2017.
- [41] J. Nelson and H. Nguyễn. Osnap: Faster numerical linear algebra algorithms via sparser subspace embeddings. In *2013 IEEE 54th Annual Symposium on Foundations of Computer Science*, pages 117–126. IEEE, 2013.
- [42] C. Paige and M. Saunders. LSQR: An Algorithm for Sparse Linear Equations and Sparse Least Squares. *ACM Transactions on Mathematical Software*, 8(1):43–71, 1982.
- [43] P. Rousseeuw and M. Hubert. Robust statistics for outlier detection. *WIREs Data Mining and Knowledge Discovery*, 1(1):73–79, 2011.
- [44] A. Rudi, D. Calandriello, L. Carratino, and L. Rosasco. On fast leverage score sampling and optimal learning. *Advances in Neural Information Processing Systems*, 31, 2018.
- [45] T. Sarlós. Improved approximation algorithms for large matrices via random projections. In *Proceedings of the 47th Annual IEEE Symposium on Foundations of Computer Science*, pages 143–152, 2006.
- [46] V. Sharan, P. Gopalan, and U. Wieder. Efficient anomaly detection via matrix sketching. *Advances in neural information processing systems*, 31, 2018.
- [47] R. Shumway and D. Stoffer. *Time Series Analysis and Its Applications: With R Examples*. Springer Texts in Statistics. Springer International Publishing, 4 edition, 2017.
- [48] A. Sobczyk and E. Gallopoulos. Estimating leverage scores via rank revealing methods and randomization. *SIAM Journal on Matrix Analysis and Applications*, 42(3):1199–1228, 2021.
- [49] J. Sybrandt, M. Shtutman, and I. Safro. Moliere: Automatic biomedical hypothesis generation system. In *Proceedings of the 23rd ACM SIGKDD international conference on knowledge discovery and data mining*, pages 1633–1642, 2017.
- [50] D. Woodruff. Sketching as a tool for numerical linear algebra. *Foundations and Trends® in Theoretical Computer Science*, 2014.

- [51] J. Yang, X. Meng, and M. W. Mahoney. Implementing randomized matrix algorithms in parallel and distributed environments. In *Proceedings of the IEEE*, pages 58–92, 2016.
- [52] Q. Zuo and H. Xiang. A quantum-inspired algorithm for approximating statistical leverage scores. *arXiv preprint arXiv:2111.08915*, 2021.